[3] Measuring Distances by Pulsed Dipolar ESR Spectroscopy: Spin-Labeled Histidine Kinases

By PETER P. BORBAT and JACK H. FREED

Abstract

Applications of dipolar ESR spectroscopy to structural biology are rapidly expanding, and it has become a useful method that is aimed at resolving protein structure and functional mechanisms. The method of pulsed dipolar ESR spectroscopy (PDS) is outlined in the first half of the chapter, and it illustrates the simplicity and potential of this developing technology with applications to various biological systems. A more detailed description is presented of the implementation of PDS to reconstruct the ternary structure of a large dimeric protein complex from *Thermotoga maritima*, formed by the histidine kinase CheA and the coupling protein CheW. This protein complex is a building block of an extensive array composed of coupled supramolecular structures assembled from CheA/CheW proteins and transmembrane signaling chemoreceptors, which make up a sensor that is key to controlling the motility in bacterial chemotaxis. The reconstruction of the CheA/CheW complex has employed several techniques, including X-ray crystallography and pulsed ESR. Emphasis is on the role of PDS, which is part of a larger effort to reconstruct the entire signaling complex, including chemoreceptor, by means of PDS structural mapping. In order to precisely establish the mode of coupling of CheW to CheA and to globally map the complex, approximately 70 distances have already been determined and processed into molecular coordinates by readily available methods of distance geometry constraints.

Introduction

An understanding of the intricate machinery of biology depends, among other things, on the knowledge of the structure and internal organization of biomolecules, cells, and tissues. The primary sources of structure at atomic resolution are, of course, X-ray crystallography and nuclear magnetic resonance (NMR), even though they are laborious and require special conditions, (as is also the case with most of the other methods). A number of other methods such as electron microscopy (EM) provide information on a coarser scale. These techniques can lead to useful insights into molecular structure, particularly when study by crystallography or NMR fails or is inapplicable. Many biomolecules are not amenable to study by NMR or crystallography for

METHODS IN ENZYMOLOGY, VOL. 423

0076-6879/07 $35.00
DOI: 10.1016/S0076-6879(07)23003-4

reasons such as insufficient quantities, inability to grow diffraction-quality crystals, large molecular weight, poor solubility, or lack of stability. The labor involved also limits the throughput. Currently, determining the structure of a relatively small membrane protein is a challenge for both NMR and crystallography; therefore, less precise methods are widely applied to gain insight into the structure and functional mechanisms. Among them, to name a few, are FRET, chemical cross-linking, ESR nitroxide scan, and cryo-EM.

Since the late 1990s, applications of both pulsed and continuous-wave (cw) Electron Spin Resonance (ESR) techniques to structure determination have grown (Banham *et al.*, 2006; Bennati *et al.*, 2005; Biglino *et al.*, 2006; Borbat *et al.*, 2002, 2004, 2006; Borovykh *et al.*, 2006; Cai *et al.*, 2006; Denysenkov *et al.*, 2006; Dzikovski *et al.*, 2004; Fafarman *et al.*, 2007; Fu *et al.*, 2003; Hilger *et al.*, 2005; Jeschke *et al.*, 2004c; Milov *et al.*, 1999, 2003a, 2005; Ottemann *et al.*, 1999; Park *et al.*, 2006; Schiemann *et al.*, 2004; Xiao *et al.*, 2001; Xu *et al.*, 2006; Zhou *et al.*, 2005). This has followed the development of the site-directed spin-labeling (SDSL) methodology (Altenbach *et al.*, 1989, 1990; Cornish *et al.*, 1994; Farahbakhsh *et al.*, 1992; Hubbell and Altenbach, 1994), wherein nitroxide labels are introduced at the desired location in proteins, as well as efforts by leading research groups to develop, perfect, and disseminate the modern ESR techniques. The application of ESR methods has also benefited from the commercialization of pulse ESR instrumentation.

The nitroxide labels typically serve as the reporter groups, providing insights about their environments such as their polarity and their solvent, and oxygen accessibility. Most important in the context of this chapter is measurement of distances between the spin labels. The SDSL-based ESR distance measurement techniques resemble FRET, but have several important advantages, such as the relatively small label size and the less perturbing nature of the nitroxide side chains (cf. Fig. 1). Furthermore, the labels are relatively easy to introduce and they provide reasonably accurate distance constraints. The notable virtues of ESR-based methods compared to X-ray and NMR methods are that the former require only tiny amounts (nano- to picomole; Klug *et al.*, 2005) of proteins (or other biomolecules), and they can be studied in a variety of environments, such as dilute solutions, micelles, lipid vesicles, native membranes, and supported lipid bilayers. There is no need to grow crystals or be concerned with long-term protein stability at high concentrations. Large biomolecules or complexes that are beyond the range of NMR or X-ray methods are not a major limitation; even unstable or transient biomolecules can be captured and studied.[1]

[1] Although solid state NMR, in particular, enhanced by DNP, should also be appreciated in this context.

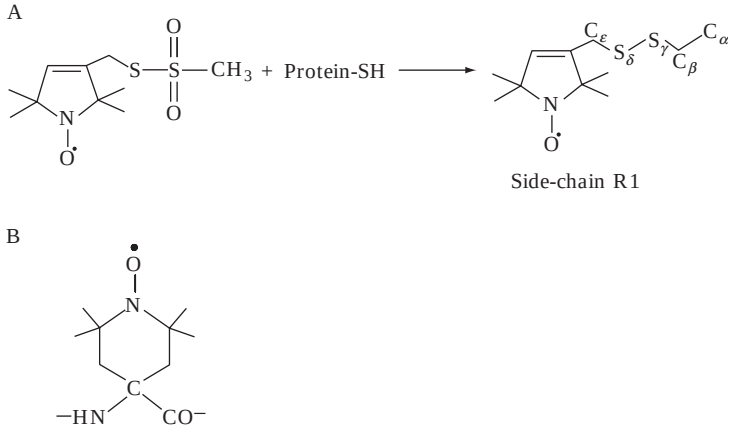

FIG. 1. (A) Protein spin labeling with MTSSL; (B) TOAC spin label.

SDSL combined with cw ESR has been routinely used for nitroxide scans (Altenbach *et al.*, 1989; Crane *et al.*, 2005; Cuello *et al.*, 2004; Dong *et al.*, 2005; Hubbell and Altenbach, 1994), providing insights into the structure and functional mechanisms of water-soluble and membrane proteins and their complexes. Double-labeling combined with pulsed ESR is currently able to readily deliver accurate long-distance constraints in a distance range of 10 to 80 Å. Such constraints may then be used to orient and dock proteins, yielding useful insights into the structure of a protein or a protein complex. They can also aid in refinement of NMR data. We refer to this emerging methodology as ''pulsed dipolar (ESR) spectroscopy,'' or PDS for short. It is the subject of this chapter.

Another notable advantage of ESR is its ability to deal with membrane proteins in their natural environments and to accommodate large protein or protein–RNA complexes composed of several proteins or RNAs. Long-distance constraints hold promise in oligonucleotide study, where they could be used in conjunction with NOE constraints and RDC to refine the structure by reducing the error that accumulates from structure determination based on a large number of short-range constraints (Borbat *et al.*, 2004).

One should, of course, note that FRET provides distances over a comparable range. Its very high sensitivity, access to longer distances, and ability to operate at biological temperatures makes it a very potent tool, but PDS has its distinct virtues. It has now become routine to express, purify, and spin-label dozens of mutants for nitroxide scan (Crane *et al.*, 2005; Cuello *et al.*, 2004; Dong *et al.*, 2005) or to produce and label a set of

cysteine double-mutants for distance measurements. The distance between nitroxides is more accurately determined than between chromophores, since it is directly obtained from a simple frequency measurement, and there are no uncertainties in κ^2 as there are in FRET. The reporter group, which is often a methanethiosulfonate spin label (MTSSL), in most cases, introduces only a small (if any) perturbation to the protein structure and functions. Since the nitroxide side-chains are smaller in size than most fluorescent labels, the uncertainty of their positions relative to the backbone is less. A drawback of PDS, as well as of FRET, is that a limited number of constraints, which are themselves the distances between the reporter groups rather than the backbone C_α carbons, may provide only limited insights into the structure. However, the detailed 3D structure is not always required to elucidate the functional mechanism. (Just the fact that the proteins are interacting or how they interact may be all that is sought in many cases.) But the fact that the distances are measured between the reporter groups does lead to a challenge in translating them into distances between the C_α carbons at the labeled sites. Modeling efforts to overcome this are in early stages of development (Bowers *et al.*, 2000); however, future developments of PDS and software tools may improve this situation.

Dipolar ESR Spectroscopy

Background

Both cw and pulsed ESR have been extensively applied to biological problems in the context of molecular dynamics (Borbat *et al.*, 2001; Columbus and Hubbell, 2002; Fanucci and Cafiso, 2006; Freed, 2000) and are now increasingly applied to distance measurements. The method of distance measurements by pulsed double electron-electron resonance (DEER, also known as PELDOR) (Larsen and Singel, 1993; Milov *et al.*, 1981, 1998; Pfannebecker *et al.*, 1996) was introduced more than two decades ago to circumvent multiple problems met in efforts to isolate weak electron–electron dipolar couplings from electron–spin–echo decays, which are usually dominated by relaxation and nuclear modulation effects (Raitsimring and Salikhov, 1985; Salikhov *et al.*, 1981). Since then, several other pulsed methods of distance measurements were introduced (Borbat and Freed, 1999, 2000; Jeschke *et al.*, 2000; Kulik *et al.*, 2001, 2002; Kurshev *et al.*, 1989; Raitsimring *et al.*, 1992); most notable is double-quantum coherence (DQC ESR, or DQC for short) (Borbat and Freed, 1999, 2000). Applications of DEER and DQC to structural problems in biology have rapidly grown in number and scope in the last few years (Borbat *et al.*, 2006; Cai *et al.*, 2006; Fafarman *et al.*, 2007; Fajer, 2005; Fanucci and Cafiso, 2006;

Jeschke *et al.*, 2004c; Milov *et al.*, 2000a, 2001; Park *et al.*, 2006; Schiemann *et al.*, 2004; Steinhoff, 2004). Whereas there are several reviews outlining ESR methods tailored to distance measurements (Berliner *et al.*, 2000; Borbat and Freed, 2000; Columbus and Hubbell, 2002; Dzuba, 2005; Fanucci and Cafiso, 2006; Freed, 2000; Jeschke, 2002; Jeschke and Spiess, 2006; Milov *et al.*, 1998; Prisner *et al.*, 2001), we have made this chapter self-contained, both providing background and emphasizing the latest developments, with a focus on illustrating the methodology through examples taken from our laboratory.

Distance Measurements by ESR

The ESR distance measurements described in this chapter are conducted in low-temperature frozen solutions with the use of nitroxide spin labels. They are based on determining the magnitude of the static dipole–dipole couplings between the spins of unpaired electrons localized on p-π orbitals of the NO groups of the nitroxides. The magnetic moments $\mathbf{m}_{1,2}$ of two electron spins 1 and 2, separated by the distance $r = |\mathbf{R}_{12}|$, interact through space via the electron spin dipole–dipole interaction

$$H_{dd} = \frac{\mathbf{m}_1 \cdot \mathbf{m}_2}{r^3} - \frac{3(\mathbf{m}_1 \cdot \mathbf{R}_{12})(\mathbf{m}_2 \cdot \mathbf{R}_{12})}{r^5} \tag{1}$$

The electron spin magnetic moment $\mathbf{m}_i$ is given by:

$$\mathbf{m}_i = \gamma_e \hbar \mathbf{S}_i \tag{2}$$

Where $\mathbf{S}_i$ is the electron spin operator for the i$^{\text{th}}$ spin, γ_e is the gyromagnetic ratio of an electron spin, and $\hbar$ is Planck's constant divided by 2π. Eq. (1) may be rewritten as:

$$H_{dd}/\hbar = \frac{\gamma_e^2 \hbar}{r^3}(3\cos^2\theta - 1)[S_{1z}S_{2z} - \frac{1}{4}(S_1^+ S_2^- + S_1^- S_2^+)] \tag{3}$$

which is valid in high magnetic fields, where the nonsecular terms (not shown) are unimportant (Abragam, 1961). One usually uses the point dipole approximation in employing Eq. (3), that is, the electron spins are far enough apart that their distributions (in, e.g., nitroxide p-π orbitals) are unimportant ($r > 5$ Å for nitroxides).[2] In Eq. (3), θ is the angle between the direction of the large dc magnetic field $\mathbf{B}_0$ and $\mathbf{R}_{12}$ (cf. Fig. 2). The term in $S_{1z}S_{2z}$ in Eq. (3) is known as the secular term, and that in the $S_1^{\pm}S_2^{\pm}$

[2] An asymmetry parameter may be necessary in the case of delocalized spin density, for example, for closely situated spatially confined tyrosyl radicals, giving rise to a slightly rhombic spectral shape (Jeschke and Spiess, 2006).

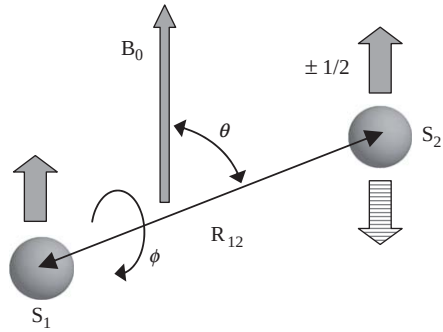

FIG. 2. A pair of electron spins S_1 and S_2 coupled via electron spin dipole–dipole interaction. Vector R_{12} connecting spins is directed along z-axis in the molecular frame of reference. In this molecular frame, the direction of the static magnetic field B_0 is determined by Euler angles $(0,\theta,\varphi)$. In DEER, spin 2 (the B-spin) is selectively flipped by the pumping pulse, changing the sign of its magnetic interaction with spin 1 (A-spin).

pseudosecular term. If, in the absence of the dipolar coupling of Eq. (3), the two electron spins have resonance frequencies ω_1 and ω_2, then the dipolar coupling in frequency units is written as

$$A(r,\theta) = \omega_d(1 - 3\cos^2\theta) \tag{4}$$

with

$$\omega_d = \gamma_e^2\hbar/r^3 \tag{5}$$

For the case of unlike spins, such as $\omega_d \ll |\omega_1 - \omega_2|$, the resonant frequency of each spin is split into a doublet separated by $|A|$; the precise value of A depends on the angle θ, yielding a range of values of A from $-2\omega_d$ to $+\omega_d$. The pulsed dipolar spectrum provides this splitting, which is shown in Fig. 3C as a function of the angle θ, obtained from a macroscopically aligned frozen sample. In the more typical case of an isotropic frozen sample, one observes an average over θ, which yields a distinct dipolar spectrum, known as a Pake doublet[3] (Pake, 1948), (cf. Fig. 3A). It shows a prominent splitting of ω_d, corresponding to $\theta = 90°$, and another splitting of $2\omega_d$, corresponding to $\theta = 0°$. The distance r is immediately and accurately obtained from a measurement of ω_d.

[3] Note that the use of spin echoes cancels the effects of hyperfine and g-tensors, so even when the two nitroxides in a given bilabeled molecule resonate at two different frequencies because of different orientations and/or magnetic quantum numbers, they still yield a single Pake doublet, resulting from their common dipolar interaction.

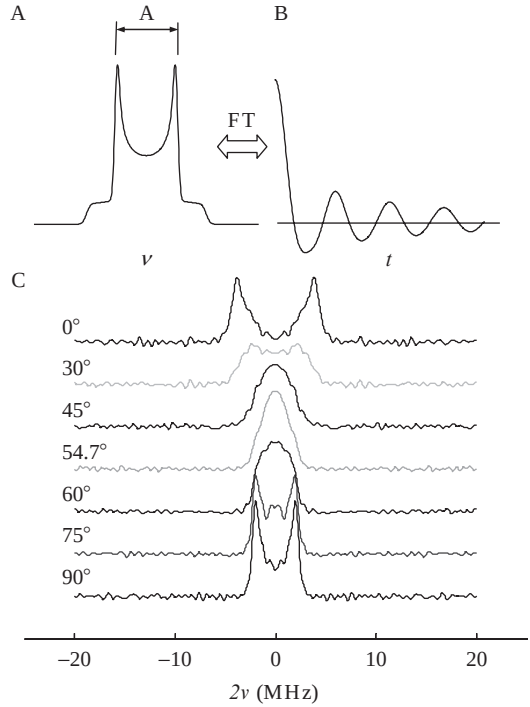

FIG. 3. (A) A dipolar spectrum in isotropic media (Pake doublet) obtained by Fourier transformation of the time-domain (B) dipolar spectrum; (C) An experimental dipolar spectrum of spin-labeled Gramicidin A (Dzikovski *et al.*, unpublished data) obtained by 4-pulse DEER at several orientations in a macroscopically aligned lipid membrane bilayer of DMPC.

The case of unlike spins corresponds to considering only the secular term in Eq. (3) and dropping the pseudosecular term. In the case of like spins, that is, $\omega_d \gg |\omega_1 - \omega_2|$, then the pseudosecular terms become important and Eq. (5) becomes $\omega_d = 3\gamma_e^2\hbar/2r^3$. Otherwise, the results (cf. Fig. 3) are equivalent.

The intermediate case of $\omega_d \sim |\omega_1 - \omega_2|$ is more complex, and is handled by careful simulation using Eq. (3), including both secular and pseudosecular terms. In the case of nitroxide spin labels, the two nitroxide spins in a given molecule usually have their ω_1 and ω_2 substantially different. This arises from their different orientations with respect to the $\mathbf{B}_0$ field, so their effective hyperfine (*hf*) and *g* values (arising from their *hf* and *g* tensors) are different. At typical ESR frequencies, this means that the unlike spin limit is reached for approximately 20 Å (9–17 GHz ESR).

If ω_d is sufficiently large, it can be determined from the broadening of the nitroxide cw ESR spectrum (Hustedt *et al.*, 1997), but this is likely to fall into the regime where pseudosecular terms are significant. Smaller couplings, ω_d require using pulse ESR methods, as we will discuss. In all cases, accurate values of distances are produced from the measured dipolar couplings.

Applications and Modalities of Dipolar ESR Spectroscopy

Both cw (Altenbach *et al.*, 2001; Hubbell *et al.*, 2000; Hustedt *et al.*, 1997; Koteiche and Mchaourab, 1999; Mchaourab *et al.*, 1997; McNulty *et al.*, 2001) and pulsed (Banham *et al.*, 2006; Bennati *et al.*, 2005; Biglino *et al.*, 2006; Borbat and Freed, 1999; Borbat *et al.*, 2002, 2006; Dzikovski *et al.*, 2004; Fafarman *et al.*, 2007; Hilger *et al.*, 2005; Jeschke *et al.*, 2004c; Milov *et al.*, 2005; Park *et al.*, 2006; Sale *et al.*, 2005; Xu *et al.*, 2006; Zhou *et al.*, 2005) ESR methods are used to measure distances between paramagnetic species, which are usually nitroxide spin-labels. However, PDS is not limited to nitroxides; distances between radical cofactors, nitroxides, and transition metal ions, have been measured in all possible combinations (Astashkin *et al.*, 1994; Becker and Saxena, 2005; Bennati *et al.*, 2003, 2005; Biglino *et al.*, 2006; Borovykh *et al.*, 2006; Codd *et al.*, 2002; Denysenkov *et al.*, 2006; Elsaesser *et al.*, 2002; Kay *et al.*, 2006; Narr *et al.*, 2002). Taken together, cw and pulsed ESR enable the measurement of distances over the range from approximately 5 to 10 Å to nearly 80 Å, with only the shorter distances accessible to cw ESR.

Cw ESR has been most often applied to nitroxides, whose powder spectra are dominated by the inhomogeneous broadenings from nitrogen *hf* and *g*-tensors, and unresolved proton *hf* couplings. One has to extract what usually is a small broadening effect introduced by the dipole–dipole interactions between the spin labels to the nitroxide powder spectra, which is usually accomplished by spectral deconvolution (Rabenstein and Shin, 1995) or a multiple-parameter fit (Hustedt *et al.*, 1997). This requires the spectra from singly labeled species as a reference for the background broadening, which is a complication and not always an option. Incomplete spin labeling makes the task more complex (Persson *et al.*, 2001). For distances less than 15 Å, the dipolar coupling approaches other inhomogeneous spectral broadenings and then can be more easily inferred from cw ESR spectra. The case of strong dipolar coupling has been extensively utilized in cw ESR (Altenbach *et al.*, 2001; Hanson *et al.*, 1996, 1998; Hubbell *et al.*, 2000; Hustedt *et al.*, 1997; Koteiche and Mchaourab, 1999; Mchaourab *et al.*, 1997; McNulty *et al.*, 2001; Rabenstein and Shin, 1995, 1996; Xiao *et al.*, 2001), both in establishing proximity and in providing

quantitative distances (Altenbach *et al.*, 2001; Hanson *et al.*, 1996, 1998; Hustedt *et al.*, 1997; McNulty *et al.*, 2001; Rabenstein and Shin, 1995, 1996; Xiao *et al.*, 2001). Cw ESR is thus practical for short distances up to a maximum of approximately 15 to 20 Å, with the values for distances under 15 Å being more reliable.

Pulsed ESR is based on detecting a spin-echo, wherein the inhomogeneous spectral broadening cancels. Spin echo temporal evolution is governed by the weaker effects of spin relaxation, electron-electron dipolar and exchange couplings, Zeeman electron-nuclear superhyperfine and nuclear and quadrupole couplings. The dipolar and exchange coupling can be isolated from the rest by means of a suitable pulse sequence, which also helps to alleviate the problem caused by the presence of single labeled molecules. The direct signal from them is filtered out in PDS, but they do contribute to the background intermolecular dipolar signal, which is best suppressed by working at low concentrations. PDS is routinely used for distances longer than 15 Å (Banham *et al.*, 2006; Borbat *et al.*, 2002, 2004, 2006; Cai *et al.*, 2006; Jeschke, 2002; Park *et al.*, 2006), and it works well all the way down to 10 Å (Fafarman *et al.*, 2007), thus significantly overlapping with the cw ESR range, but it is much less affected by inefficient labeling and can readily yield distance distributions.

Implications of Nitroxide Label Geometry

Even though there is a rigid amino acid spin bearing label (TOAC; cf. Fig. 1), which is being used in peptide studies (McNulty *et al.*, 2001; Milov *et al.*, 2000a, 2001), currently there is no convenient way to incorporate it into proteins; consequently, a variety of cysteine-selective spin labels are in common use (Columbus *et al.*, 2001; Mchaourab *et al.*, 1999). Nitroxide label side chains are flexible and their conformational dynamics (Hustedt *et al.*, 2006; Langen *et al.*, 2000), and the volume they sample, depend on the label type and the details of the protein landscape. They usually reside on the protein surface, since it is difficult to provide efficient labeling to achieve a sizable fraction of double-labeled protein for sites that are deeply buried or in the protein core. Since the distances are measured between nitroxide NO groups rather than between backbone carbons, the side-chain length of about 7 Å causes considerable uncertainty in the C_α–C_α distances accessible by cw ESR. Several studies have attempted refinement of the side-chain geometry to improve the correlation of inter-nitroxide distances with the distances between the respective alpha-carbons (Sale *et al.*, 2002, 2005). The larger distances in the typical PDS range of 20 to 70 Å are relatively more accurate (Sale *et al.*, 2005), but efficient

methods of generating backbone constraints from a substantial set of ESR-derived distance restraints are just being developed.

Also, one observes a distribution in the distances between the two NO groups. It depends on the conformational space that the protein samples, the flexibility of the nitroxide side-chain at the particular site, and the relative orientations of the two nitroxide side-chains. Solvent-exposed sites often exhibit wide distance distributions (Borbat *et al.*, 2002; Hustedt *et al.*, 2006; Sale *et al.*, 2002). In any case, the first moments of distance distributions (the average distances) obtained from the time-domain data usually are accurate to 5 Å or better, 1 to 3 Å being typical. The distance distributions between fully or partially buried nitroxides are generally more restricted. Distances between buried radical cofactors reflect their immobilized status and the uncertainty in distance is often a fraction of an Angstrom (Bennati *et al.*, 2003; Kay *et al.*, 2006).

3-Pulse DEER

DEER[4] in its original 3-pulse form (Milov *et al.*, 1981) (also dubbed PELDOR), depicted in Fig. 4, is based on the two-pulse primary spin-echo $\pi/2$-τ-π-τ-*echo* sequence to which a third pumping π-pulse is added. The $\pi/2$ and π pulses, separated by time interval τ, are applied to spins resonating at

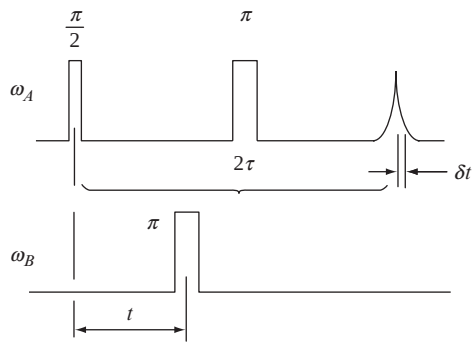

FIG. 4. The original 3-pulse form of DEER (Milov *et al.*, 1981). Primary echo is formed by $\pi/2$ and π pulse sequence at the frequency of A-spins. The pumping pulse at ω_B is applied at a variable time t to probe the dipolar coupling between A and B spins. The spectral excitations at both frequencies should not overlap, thus the pulses are made selective.

[4] Both acronyms PELDOR and DEER do not indicate the fact that they are solely concerned with dipolar couplings rather than dynamics. For this reason, we prefer to use PDS, to make explicit the function of the method and make the distinction with classic cw and pulsed ELDOR techniques.

the frequency ω_A, to form the primary echo at the time 2τ after the $\pi/2$ pulse. These spins are commonly referred to as A spins. The third (pumping) pulse is applied at the resonant frequency ω_B (at a variable time t) sufficiently different from ω_B that it does not have any direct effect on the A spins but instead inverts the spins resonating at ω_B, that is, the B spins.[5] The B spins, at a distance r from the A spins, yield the electron dipolar coupling A (cf. Eq. (4)), which splits the resonant line at ω_A into a doublet.[6] Thus, flipping the B spin inverts sign of the coupling[7] sensed by the A spin. This results in the instant shift of the Larmor precession frequency of spins A; it was shown in Milov *et al.* (1981) that the effect manifests itself as a modulation of the spin-echo amplitude, $V(t)$[8]:

$$V(t) = V_0(1 - p(1 - \cos A(r, \theta)t)) \qquad \text{for } 0 < t < \tau. \tag{6}$$

Here, V_0 is the echo amplitude in the absence of the pumping pulse, p is the probability of flipping spin B, and $A(r, \theta)$ is given by Eq. (4). Powder averaging of $V(t)$ over an isotropic distribution of orientations of $\mathbf{R}_{12}$, under the simplifying assumption of random orientation of the magnetic tensors of the A and B spins relative to $\mathbf{R}_{12}$, produces a decaying oscillatory signal (cf. Fig. 3B):

$$V(t) = V_0(1 - p(1 - v(\omega_d t))) \tag{7}$$

where

$$v(\omega_d t) = \int_0^{\pi/2} \cos[\omega_d(1 - 3\cos^2\theta)t]d(\cos\theta) \tag{8}$$

and the frequency of oscillation, $\nu_d = \omega_d/2\pi$, from which r is calculated as $r[\text{Å}] = 10(52.04/\nu_d[\text{MHz}])^{1/3}$. Cosine Fourier transformation of $v(\omega_d t)$ versus $2t$ yields the dipolar spectrum with the shape of a Pake doublet (cf. Fig. 3A). Note that, in PDS, it is customary to perform the FT versus t (with the splitting

[5] There can be more subtle effects on spin A arising from the dipolar interaction during the pulse at ω_B (Maryasov and Tsvetkov, 2000).

[6] We exclude electron exchange coupling for brevity; it is insignificant for nitroxide labels separated by r > 15Å.

[7] Of course, the A spin also splits the resonant frequency of the B spin into a doublet. A detailed consideration of the spin dynamics for a coupled spin pair (Maryasov and Tsvetkov, 2000) shows that both components of the dipolar doublet are required to be flipped by the π pulse; thus, sufficient amplitude of the microwave magnetic field acting on coupled spins be applied.

[8] The dipolar signal for $\tau < t < 2\tau$ is a repeat of the signal for $t < \tau$. Therefore, in the sequel, we shall assume that t varies only from 0 to τ .

between the singularities in the plot being twice the dipolar splitting), and often only one-half of the dipolar (symmetric) spectrum is plotted versus dipolar frequency, ν.

Eqs. (6–7) should be considered as a reasonable approximation for DEER, which is suitable for the majority of cases encountered in biological applications of PDS. In reality, a number of factors affect the signal, and their effects usually cannot be written in closed form or are unwieldy. Some will be discussed later. What is significant is that DEER achieves a good separation of the dipolar coupling from relaxation effects because the time between the $\pi/2$ and π spin-echo pulses at ω_A is constant, (i.e., τ in Fig. 4 is constant in the experiment; this is referred to as a constant time pulse sequence), and relaxation effects introduced by the pumping pulse can normally be ignored.[9] Nuclear ESEEM is also considerably suppressed but still could be an issue when p is not small.

The Newer Methods

4-Pulse DEER

The methods of 4-pulse DEER (Pannier *et al.*, 2000) and 6-pulse DQC (Borbat and Freed, 1999, 2000; Borbat *et al.*, 2001, 2002; Freed, 2000) are illustrated in Fig. 5. The 4-pulse DEER sequence is an improvement over 3-pulse DEER. It is based on the 3-pulse spin- echo sequence $\pi/2$-τ'-π-($\tau+\tau'$)-π-τ-*echo*, which refocuses the primary echo formed by the first two pulses. The additional pumping pulse at ω_B is varied in time between the π pulses at ω_A. Both τ and τ' are fixed; thus, relaxation does not modify the signal envelope recorded versus position of the pumping pulse. The signal is described by Eqs. (6–7) at the same level of approximation as 3-pulse DEER. This pulse sequence substantially simplifies its technical implementation, which has permitted commercial implementation. The pulses do not need to overlap or even come close (cf. the Some Technical Aspects of DEER and DQC section, p. 86), thereby avoiding some small but significant dead times effects in 3-pulse DEER. Also, 4-pulse DEER permits using larger B_1's than does 3-pulse DEER, at optimal settings of ω_A and ω_B, which provides greater sensitivity.

DQC

The 6-pulse DQC pulse sequence $\pi/2$-t_p-π-t_p-$\pi/2$-t_d-π-t_d-$\pi/2$-(t_m-t_p)-π-(t_m-t_p)-*echo* is based on a different principle. All pulses are applied at the same frequency ω_A, and it is important that they all be intense in order to excite the

[9] If the flip-flop rate of B spins is low, they do not introduce significant relaxation effects.

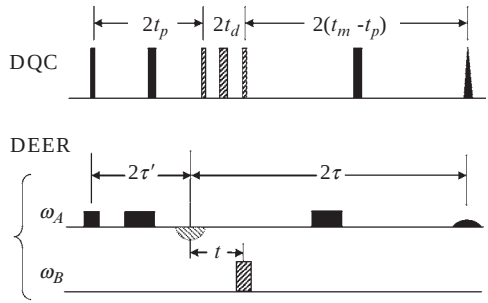

FIG. 5. 6-pulse DQC (top) and 4-pulse DEER (bottom) sequences: The DQC 6-pulse sequence (Borbat and Freed, 1999, 2000) is based on intense pulses in order to probe the dipolar coupling between (nearly) all intramolecular pairs of nitroxide spins. The first part of the sequence $\pi/2$-t_p-π-t_p is a preparation period, at the end of which an echo is formed (not observable) from the anti-phase single coherence between the two coupled spins. The third and fifth pulses ($\pi/2$) convert this coherence into double quantum coherence and then back into anti-phase single-quantum coherence (with the fourth pulse (π) refocusing the spins). This anti-phase single-quantum coherence then develops into the observable single spin coherence after the $2(t_m-t_p)$ time period. The sixth pulse (π) is applied to form an echo of this coherence. This echo is selected by phase cycling of the signal that passes through the double quantum filter (hatched). The time t_d of the 3-pulse double quantum filter is kept short and constant. The time t_m is also kept constant to minimize phase relaxation effects; and it defines the time available for dipolar evolution. The relevant time variable for observing the dipolar signal is $t_\xi \equiv t_m-2t_p$, which is zero when $t_p = t_m/2$. The pulse sequence is thus dead-time free. The reference point $t_\xi = 0$ is well-defined due to the very short pulses used in DQC.

The 4-pulse form of DEER (Jeschke, 2002; Jeschke and Spiess, 2006) is a modification of its 3-pulse predecessor. It is based on detecting the refocused primary echo formed by $\pi/2$-τ'-π-($\tau + \tau'$)-π-τ-*echo* pulse sequence at the frequency, ω_A of A-spins. The time variable t is referenced to the point where the primary echo from the first two pulses is formed (but is not detected). At $t = 0$, the dipolar phase is zero for all A spins (the precise $t = 0$ is limited by the width of the pulses). Shifting the starting point for dipolar evolution away from the second pulse by τ' makes this pulse sequence dead-time-free with respect to dipolar evolution and eases its technical implementation.

whole spectral distribution of spins, that is, all the spins are regarded as A spins (cf. Fig. 6). The first interval, $2t_p$, is used to let the normal single-quantum coherence with spin character $S_{1y} + S_{2y}$ evolve into what is known as anti-phase single-quantum coherence between the coupled spins with spin character $S_{1x}S_{2z} + S_{2x}S_{1z}$. Then, the $\pi/2$-t_d-π-t_d-$\pi/2$ pulse ''sandwich'' (hatched bars in Fig. 5) converts this coherence into double-quantum coherence with spin character $S_{1x}S_{2y} + S_{1y}S_{2x}$ (by means of the first $\pi/2$ pulse), then refocuses it by means of the π-pulse, only to convert it back to (unobservable) anti-phase coherence (by means of the last $\pi/2$ pulse), which evolves back into the observable coherence $S_{1y} + S_{2y}$, giving rise to the echo. Both spins participate equally in the process. The first and the last π-pulses of the 6-pulse sequence

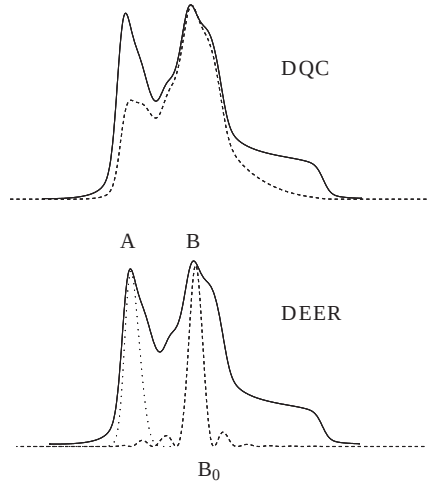

FIG. 6. Excitation of the nitroxide spectrum at 17.3 GHz in the microwave Ku band for DQC (top) and 3-pulse DEER (bottom). The ^{14}N nitroxide ESR spectrum is plotted as a solid line and the spectral excitation profiles are plotted as dashed lines. The detection frequency in DEER is set at the low field edge of the spectrum (A) and the pump pulse frequency corresponds to positioning it at the center (B). The pumping pulse is 4 G (45 ns π pulse) in DEER. The DQC excitation profile corresponds to a 48 G (3.7 ns) π pulse.

are used to refocus in-phase and anti-phase coherences, thereby respectively enhancing the effectiveness of the double-quantum sandwich and producing the echo at time $2t_m + 2t_d$. The signal in the ideal limiting case of intense and nonselective pulses can be written as seen in Eq. (9) (Borbat and Freed, 1999, 2000).

$$\begin{aligned} V &= -V_0\,[\sin A(r,\theta)t_p]\sin[A(r,\theta)(t_m - t_p)] \\ &= \frac{V_0}{2}[\cos A(r,\theta)t_m - \cos\, A(r,\theta)t_\xi] \end{aligned} \tag{9}$$

The signal is recorded versus $t_\xi - t_m - 2t_p$, with t_m kept constant in order to keep relaxation effects (which decay exponentially in time) constant. Powder averaging gives

$$V = \frac{V_0}{2}[v(\omega_d, t_m) - v(\omega_d, t_\xi)] \tag{10}$$

with $v(\omega_d, t_\xi)$ as given by Eq. (8). For large $\omega_d t_\mathrm{m}$, the first term in Eq. (10), which is constant in t_ξ, is close to zero.

The important feature of the double quantum coherence sandwich is that it very effectively filters out the single quantum signal arising from the

individual spins, and only passes the signal from the interacting part of the two spins, which contain only the dipolar oscillations. The only background that can develop is from the double quantum coherence signal that originates from the bath of surrounding spins, that is, from intermolecular dipolar interactions with other doubly labeled molecules (and singly labeled molecules when they are present). The signal envelope $V(t_\xi)$ is symmetric with respect to $t_\xi = 0$ (cf. Fig. 7). This is referred to as being dead-time free, since the dipolar oscillations are a maximum at $t_\xi = 0$ (cf. cosine term in Eq. (9)). This also means that it is sufficient to collect the data points for $t_\xi \geq 0$. There is, however, an apparent dead-time, which is determined by the pulse width; it typically is a few nanoseconds.

Relaxation effects that decay exponentially but nonlinearly in time in the exponent (Borbat *et al.*, 2002), or substantial differences in T_2's from the two spins, can modify the signal. The 6-pulse sequence generates a number of echoes, but with the proper phase cycling, only the dipolar modulation of the double-quantum filtered echo is detected. The details can be found in Borbat and Freed (2000).

The DQC experiment maintains phase coherence between the two coupled spins and treats them equally, whereas in DEER, phase coherence between the two coupled spins is of no importance. The independence

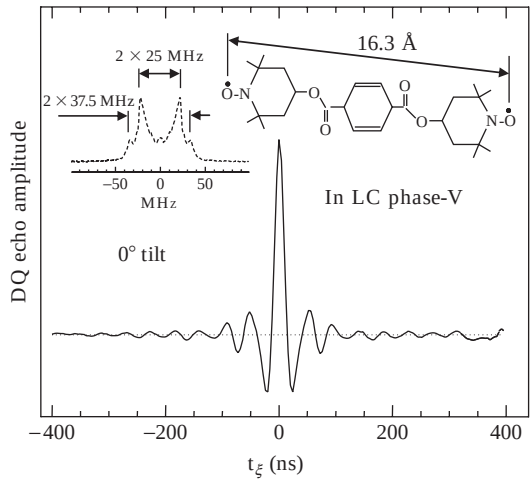

FIG. 7. 17.4 GHz DQC from a 16.3 Å rigid biradical aligned in LC phase-V (Borbat and Freed, 2000). The LC director is oriented parallel to $\mathbf{B}_0$. The dipolar coupling is ~25 MHz with maximum outer splitting of ~37.5 MHz due to pseudosecular term.

of tuning of the pulse conditions at both frequencies, as well as its applicability to widely separated spectra, makes the DEER sequence quite flexible. Nevertheless, it can be shown that the dipolar signal recorded in DEER is based on the same type of evolution of in-phase and anti-phase coherences as in DQC (Borbat and Freed, 2000). This is also the case with other related pulse sequences (Borbat and Freed, 2000). Although it may look complex, the DQC experiment, once it is set up, is rather simple to use. The similarity in DQC and DEER means that the maximum useful time of the experiment ($2t_m$) in DQC and 2τ in DEER will be comparable, except for respective differences in signal-to-noise ratio (SNR), as will be discussed.

DQC and DEER have proven to be the most useful methods, and together they address a wide range of applications. (Figs. 9, 10, 11, 14, 16, and 21 show examples of DQC and 4-pulse DEER signals.)

Other Methods

Several other pulse sequences for PDS with useful features have been introduced (Borbat and Freed, 2000; Jeschke *et al.*, 2000; Kulik *et al.*, 2001; Kurshev *et al.*, 1989; Raitsimring *et al.*, 1992). They are related in one way or another to DEER or DQC, since they are all based on dipolar evolution of single quantum in-phase and anti-phase coherence, and some try to minimize relaxation effects based on constant time pulse sequences. They have not been extensively used because of various shortcomings. Additional methods are based on the dipolar contribution to spin relaxation, so they are not as able to provide accurate distances, but they can be useful. The reader is referred to Raitsimring and Salikhov, 1985; Rakowsky *et al.*, 1998; Seiter *et al.*, 1998.

Intermolecular Effects, Clusters, Oligomers, and Spin-Counting

Eqs. (6) and (7) describe the dipolar signal in DEER originating from a pair of spins A and B. The signal from the A and B spins in each (doubly labeled) molecule is usually the signal of interest. All the other A (resonating at ω_A) and B (resonating at ω_B) spins in the sample also contribute to the DEER signal. For example, they represent the intermolecular dipolar interactions. The simplest intermolecular case that can be represented in closed form is the case of uniform spatial spin distribution over an isotropic magnetically dilute sample. Since the dipolar interaction in this case is weak, it can be represented by the secular term in Eq. (3). Then, the effect of all the other B spins on the ith spin, A, is multiplicative, given by the product obtained in Eq. (11) (Milov *et al.*, 1984).

$$V_{i,inter}(t) = \left\langle \prod_{j\neq i}^{N-1} [1 - p_{ij}(1 - \cos A(\mathbf{r}_{ij})t)] \right\rangle. \quad (11)$$

Here, N is the number of spins in the sample. Angular brackets denote averaging over all possible configurations of N spins $\{\mathbf{r}_{ij},...,\mathbf{r}_{Nj}\}$. Averaging by the Markov method (Chandrasekar, 1943) leads to a simple exponential decay

$$V_{i,inter}(t) = \exp(-kt) \quad (12)$$

with

$$k^{-1} = 1.0027 \frac{10^{-3}}{pC} \quad (13)$$

where C is the molar concentration and p is the probability of flipping B spins by the pumping pulse (typically, 0.1–0.3). The dipolar signal from the spin pair of interest (cf. Eq. (7)) is then modified by multiplication by this decaying factor, (cf. Figs. 8, 9, and 13a for additional examples). A similar mechanism works among A spins, and is known as the instantaneous diffusion (ID) mechanism (Klauder and Anderson, 1962; Nevzorov and Freed, 2001a; Raitsimring *et al.*, 1974; Salikhov *et al.*, 1981), which, unlike ordinary relaxation mechanisms, can be partially refocused (Slichter, 1990).

A similar approach can be applied to an isotropic uniform distribution in space with fractal dimensionality, where a closed-form solution can be

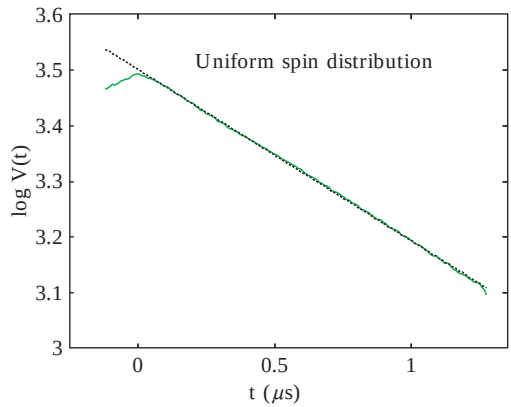

FIG. 8. An example of 4-pulse DEER (solid line) from a uniform distribution of spins in an isotropic sample illustrates the intermolecular signal given by Eq. (12). Dashed line is a fit to the straight line in the logarithmic plot. To achieve the uniform spin distribution, 0.01 mole percent of spin-labeled alamethicin was magnetically diluted with WT by a factor of 20 to avoid effects of its aggregation (unpublished, this lab).

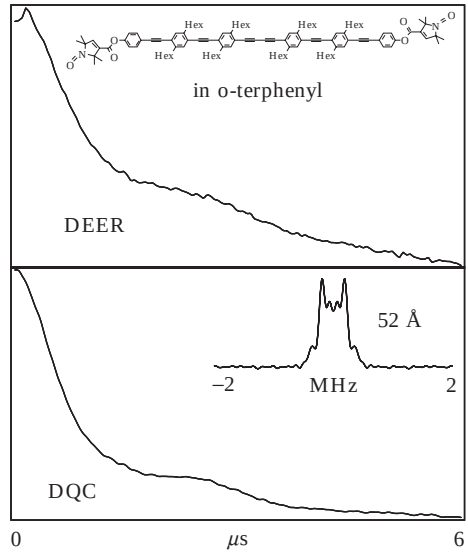

FIG. 9. Long rigid biradical in o-terphenyl glass at 50 K. DQC (bottom) shows a stronger signal than DEER (top) due to strong pulses and partial suppression of nuclear spin diffusion of DQC. The signal profile in DQC is, however, more affected by spin relaxation that decays according to a t^2 dependence in the exponent (Borbat *et al.*, 2002). (Just the oscillating part of the full DEER signal is shown for better comparison of the two signals.) (Unpublished, rigid rod biradical, courtesy of G. Jeschke).

written (Milov and Tsvetkov, 1997). Practical examples of lower dimension are the 2D case of unilamellar lipid membranes or the 1D case of self-avoiding polymer chains.[10] Note that we can distinguish two types of heterogeneous sample—microscopic or macroscopic (Jeschke and Schlick, 2006). This can be understood by realizing that spins beyond a certain radius, call it $R_{inter}(t_m)$, make a negligible contribution to Eq. (11) or (12) (Jeschke *et al.*, 2002). Therefore, such a length scale, R_{inter} can be used to separate micro- and macroscopic domains. Macroscopic heterogeneity represents variations over length scale greater than R_{inter} in concentration or composition throughout the sample (and it also includes pulse amplitude variation over the sample). The signal given by Eqs. (12) and (13) is simply averaged over the sample. Micro-heterogeneous systems such as lipid membranes or clusters, which have characteristic microscopic order, are usually not amenable to simple analytic solutions, and their signals should

[10] These are not exactly fractal cases and they are not described as in Milov and Tsvetkov (1997), but have similar time dependence.

be derived based on the appropriate averaging of Eq. (11) for the particular case. Good approximations are possible but are beyond the scope of this chapter. In general, the dipolar signal is modified, and there can be a large nonlinear background, which needs to be accounted for, or else removed to isolate the informative part of the signal $V(Wd,t)$ (cf. Eq. 8) (Borbat *et al.*, 2002; Jeschke, 2002; Maryasov *et al.*, 1998).

The case of a small group of spins (clusters) has been considered in the literature (Milov *et al.*, 1984, 2000b, 2003b; Raitsimring and Salikhov, 1985; Ruthstein *et al.*, 2005; Salikhov *et al.*, 1981). This case requires numerical treatment based on Eq. (11), typically by the Monte Carlo method, although simplified approaches exist and were used to roughly estimate the number of spins in a cluster (Milov *et al.*, 1984). In fact, an accurate treatment is rarely justified in such cases, since there are too many unknown parameters to fit and realistic data permit determining one or two parameters at most. In addition, one must have a priori knowledge about the system in order to model it properly.

We note that a generalization of DQC methods to provide multiple-quantum coherence selective pulses is, in principle, possible (Borbat and Freed, 2000). Such a methodology would be very useful for spin counting, but it has not yet been developed for practical use in ESR.

From the standpoint of PDS, the intermolecular term is usually an unwanted complication, requiring that the intramolecular signal of interest be separated from the intermolecular contribution to the signal. Clearly, the best approach is to minimize the latter by sample dilution, whenever it is an option and sensitivity permits.

For the sophisticated pulse sequence of DQC, there is no rigorous theory for the intermolecular dipolar effects in DQC. However, when pulses are strong and the system is sufficiently dilute, the intramolecular dipolar signal is relatively less affected than in DEER by other spins (cf. Fig. 7). Therefore, at low concentrations, DQC has the advantages of better sensitivity due to all or nearly all the spins participating and weaker effects of surrounding spins. In cases of high local concentrations (lipid vesicles, protein oligomers, or peptide clusters), DEER is able to produce the same (or sometimes even better) sensitivity than DQC because of reduced ID from the weaker DEER pulses. Some examples of dilute samples where DQC works better are shown in Figs. 9 and 10.

Data Processing in DQC and DEER

An example of a typical DEER signal from a spin-labeled protein is shown in Fig. 11 and that for a case of a small cluster in Fig. 12. DQC signals are shown in Fig. 7 (cf. also Figs. 14, 16B, and 21A). For DQC, first, the

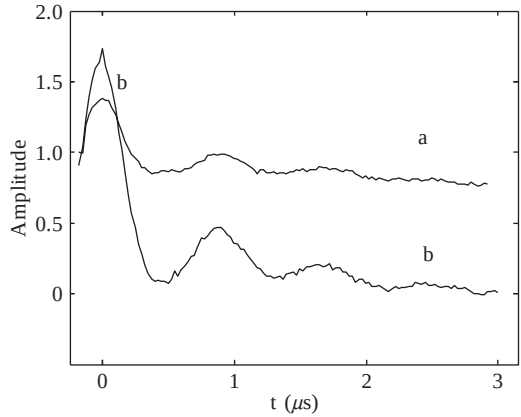

FIG. 10. Comparison of the DQC signal versus t_ξ (b) and the 4-pulse DEER versus t (a) operating at 17.4 GHz for spin-label at position 340 in the cytoplasmic domain of band 3 protein (Zhou *et al.*, 2005). The same resonator and sample was used in both cases, data collection time was 25 min, T was 70 K. In DQC 9 ns π pulses (20 Gauss B_1) were used; 16/32/32 ns observing pulses and 28 ns pumping pulse were used in DEER. SNR of DQC is 142, in DEER it is 43. The DQC SNR may be improved by using shorter π pulses. An additional advantage of DQC was due to its partial cancellation of nuclear spin diffusion (cf. Sensitivity of PDS section, p. 79). [Current operating performance for these conditions (and for the data of Fig. 9) yields SNRs that are greater by a factor of 2.5.] (unpublished data; the protein courtesy of Zheng Zhou).

intermolecular background signal is removed by means of least square polynomial fitting in the time-domain of the latter part of the signal; then, this is extrapolated back to the earlier part of the signal and subtracted out (Borbat *et al.*, 2002). In the case of DEER, the removal of background signal often is performed by fitting the latter part of the signal to a straight line in a log plot under the assumption of an exponent that is linear in time in Eq. (12). When this is not the case, a low-degree polynomial can be used instead. Another way of accounting for the intermolecular background is to use methods of signal reconstruction with simultaneous baseline fitting (cf. the Distance Distributions section, p. 73). This method separates out the part of the signal governed by the intramolecular kernel (see the following text). Using a more dilute sample is recommended when possible since it reduces background and also helps to arrive at a more linear background. Spectral overlap of pulse excitations at the two frequencies in DEER, which can arise when using a stronger pumping pulse to increase p and thereby to enhance the signal, complicates the signal and its analysis due to unwanted effects (cf. Fig. 21B). In the case of a heterogeneous system, one could first study a reference sample with the same spin

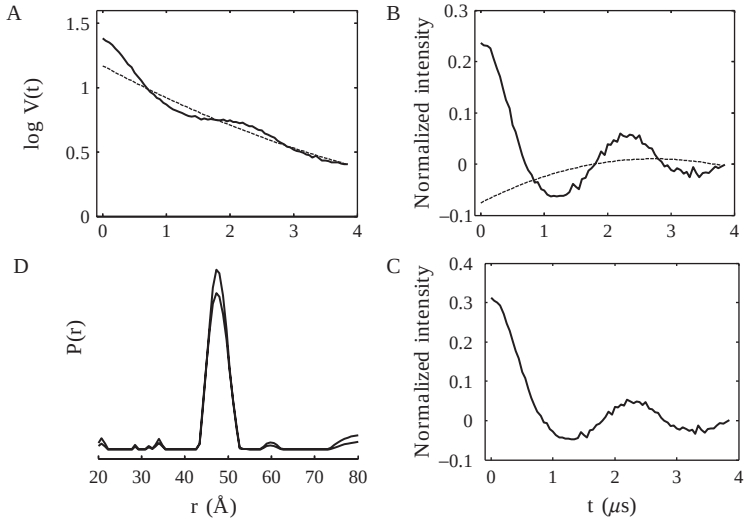

FIG. 11. Data processing of Ku band time-domain DEER signal for nitroxide labeled monoamine oxidase reconstituted in detergent micelles. (A) The intermolecular background is removed by first fitting the data from 1 to 4 μs to a second-degree polynomial (rather than to a straight line, as relevant to this case) in the log plot, followed by subtracting it out. (B) Dipolar signal after removal of background. Dashed line shows the correction for the background that was generated in the process of MEM reconstruction (Chiang *et al.*, 2005b). (C) Corrected dipolar signal generated by fitting (A) to a linear background signal; it is indistinguishable from (B), indicating the capability of MEM to separate out the inter- and intramolecular contributions to the dipolar signal in this example. (D) $P(r)$'s produced from data from (B) (upper curve) and (C). The very small peaks are caused by noise and signal distortions (mostly caused by using a short pump pulse of 20 ns). (Unpublished, this lab; protein sample provided by A. Upadhyay.)

concentration but with singly labeled molecules or spin probes in order to determine the shape of the intermolecular signal. (But this method has limited applicability and polynomial fitting is usually the method of choice.)

Extracting Distance and Spin-Count Information

The average distance can to good accuracy be extracted by inverse reconstruction (see the Distance Distributions section, p. 73) (Bowman *et al.*, 2004; Chiang *et al.*, 2005a,b; Jeschke *et al.*, 2002, 2004b) of the intramolecular signal obtained from the experimental data (Borbat *et al.*, 2002; Milov *et al.*, 1999); or from analyzing the signal with parameterized geometrical modeling (Borbat *et al.*, 2002); or from the singularities or the half-width of the dipolar spectrum (Park *et al.*, 2006); or simply by an estimate based on temporal envelope (Milov *et al.*, 1999; Park *et al.*, 2006).

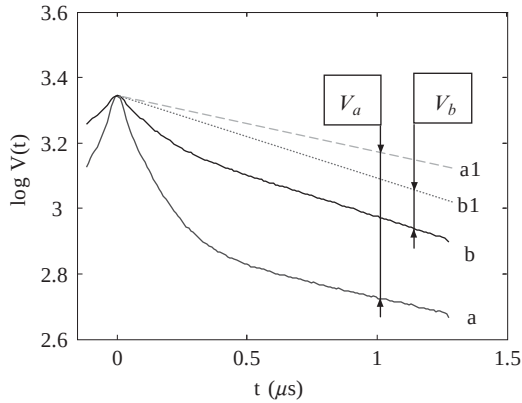

FIG. 12. The DEER signal in the case of clusters for the system of Fig. 8 but less magnetically diluted (b) than in Fig. 8, and without dilution (a). (a1, b1) are straight line fits to the asymptotic parts of (a, b). (a) is typical for a spin cluster; in this case, single-labeled alamethicin molecules are organized into small clusters with expected constant number of monomers. (b) represents the same spin concentration but magnetically diluted by a factor of 5 with unlabeled peptide, indicating that this signal indeed originates from a spin cluster. The asymptotic DEER amplitudes (V_a, V_b) can be immediately analyzed to yield an estimate of how many peptide molecules, N, are in the cluster (Milov *et al.*, 1984), given that the fraction of peptides in clusters is known. Based on Milov *et al.* (1984) $\ln V_a = (N-1)\ln(1-p)$, where p (cf. Eq. (7)) was 0.2. This yields four peptide molecules per cluster. (Unpublished, this lab.)

The latter includes using the period of oscillation or half-width of the initial decay (ca. $2\pi/5\omega_d$). For very long distances, when it is known a priori that there should be a reasonably well-defined distance, access to a fraction of the dipolar oscillation period suffices but requires prediction of the baseline or knowledge of p (in the case of DEER) and spin labeling efficiency. The error in distance, even with such crude methods, is relatively small (*vide infra*) due to the inverse cubic dependence of the ω_d on the distance, so it does not normally exceed the uncertainties introduced by the nitroxide side-chains.

For clusters, controlled magnetic dilution proved useful to detect aggregation and evaluate the size of clusters and number of spins (Milov *et al.*, 1999). We illustrate in Fig. 12 the practical implementation of the method, with some additional details given in Milov *et al.* (1984).

Distance Distributions

Several approaches to determining distance distributions of paramagnetic centers in solids were utilized in the early applications of DEER and related methods (Milov *et al.*, 1981; Pusep and Shokhirev, 1984;

Raitsimring and Salikhov, 1985). Such methods have been improved (Bowman *et al.*, 2004; Chiang *et al.*, 2005a,b; Jeschke *et al.*, 2002, 2004b) and the Tikhonov regularization method is now a workhorse for extracting distance distributions from the raw or preprocessed data.

The time-domain dipolar signal may generally be viewed as $V_{intra}\,A_{inter} + B_{inter}$ (B_{inter} originates from singly labeled molecules and, for uniform spin distributions in the sample, its time dependence is given by A_{inter});[11] the A and B terms are removed to the extent possible; and then, what is taken to be a reasonably accurate representation of V_{intra} is subject to inverse reconstruction by Tikhonov regularization or related methods. The problem can be represented by a Fredholm integral equation of the first kind,

$$V_{intra}(t) = V_0 \int_0^\infty P(r)K(r,t)dr \tag{14}$$

with the kernel $K(r,t)$ for an isotropic sample (cf. Eqs. (4–5)) given by

$$K(r,t) = \int_0^1 \cos\left[\omega_d t(1-3u^2)\right]du \tag{15}$$

The inversion of the signal V_{intra} given by Eq. (14) to obtain $P(r)$, the distance distribution, is, in principle, achievable by standard numerical methods, such as singular value decomposition (SVD), but it is an ill-posed problem that requires regularization methods in order to arrive at a stable solution for $P(r)$. In the practical implementation, the data are discrete and available over a limited time interval, and the actual form of the kernel $K(r,t)$ may differ from the ideal form given by Eq. (15).

Tikhonov regularization (Chiang *et al.*, 2005a,b; Jeschke *et al.*, 2004b) recovers the full distribution in distance, $P(r)$. It is based on seeking an optimum, $P(r)$, which tries to minimize the residual norm of the fit to the data while also trying to maximize the stability of $P(r)$ (to reduce its oscillations). The relative importance of both is determined by the regularization parameter, λ. The L-curve method for optimizing λ is computationally very efficient and the most reliable to date. In the Tikhonov method, the regularization removes the contributions of the small singular values, σ_i in the SVD that are corrupted by the noise by introducing the filter function,

[11] But B_{inter} is not, in general, the same as A_{inter} for the case of micro-heterogeneity, wherein the local spin concentration determines B_{inter}.

$$f_i \equiv \frac{\sigma_i^2}{\sigma_i^2 + \lambda^2} \tag{16}$$

which filters out those contributions for which $\sigma_i^2 \ll \lambda^2$. Further refinement of the $P(r)$ can be performed by means of the maximum entropy method (MEM) (Chiang *et al.*, 2005b), although it is computationally more time-consuming. The latest versions of MEM and Tikhonov regularization permit one to simultaneously fit and remove the effects of A_{inter} and/or B_{inter} while optimizing the $P(r)$ from raw experimental data[12] (Chiang *et al.*, 2005b).

Experimental artifacts, signal distortions, and residual baseline make signal recovery somewhat less accurate than what has been demonstrated on model data that were generated using the ideal kernel of Eq. (15). The test examples of Fig. 13 demonstrate the accuracy of recovery of average distances and distribution widths when the signal is free of artifacts. It is clear that with a good SNR, average distances of the order of 80 Å can be obtained. Very long distances can be recovered, given undistorted and good SNR data. Figure 11 demonstrates the application to real data with baseline correction by MEM.

Relaxation

The amplitude of the primary echo V_0 decays with increasing pulse separation, τ (cf. Fig. 4) due to phase relaxation. Therefore, the maximum dipolar evolution time interval, t_{max} available for recording $V(t)$ is ultimately limited by the phase memory time, T_m (or T_2). In the simplest case, $V(t) = V_0 \propto \exp(-2t/T_m)$. This limits the maximum distance, r_{max} that one can measure, over a reasonable period of signal averaging. Depending on the signal strength, t_{max} is approximately 1 to 3 T_m and cannot be extended much further. Here, t_{max} is essentially $2t_m$ in DQC and $2(\tau' + \tau)$ in DEER (cf. Fig. 5). The largest measurable distance r_{max} is proportional to ${t_{max}}^{1/3}$ in order to recover the dipolar oscillation (Borbat and Freed, 2000). Thus, only a minor increase in r_{max} could be made by increasing t_{max}, and this would necessarily require a large increase in signal averaging. For nitroxide-labeled proteins, T_m is largely determined by the dynamics of the nearby protons (Huber *et al.*, 2001; Lindgren *et al.*, 1997; Zecevic *et al.*, 1998), especially those from methyl groups, leading to the simple exponential decay expressed above with T_m in the range of 1 to 2 μs for buried or partially buried labels. Such relaxation times are typical for hydrophobic environments that are encountered in lipid membranes (Bartucci *et al.*, 2006) and the protein interior (Lindgren *et al.*, 1997). This permits an r_{max}

[12] Available for download through the ACERT web page www.acert.cornell.edu.

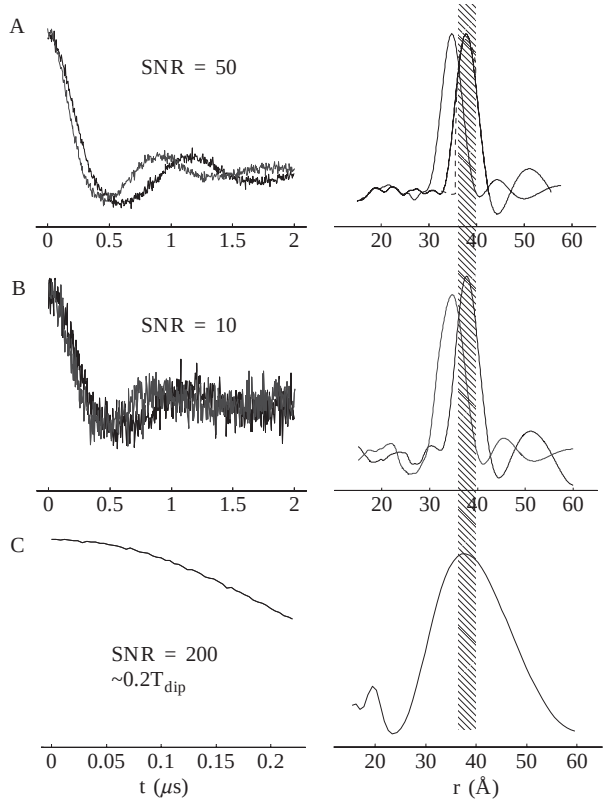

FIG. 13. (A,B) Simulated dipolar signals for two distances of 35 and 38 Å, both rms widths of 3.6 Å, for different levels of noise. Left panels show time-domain signals, and the right panels show distance distributions, $P(r)$ reconstructed using L-curve Tikhonov regularization. Note that just a 3 Å difference produces distinct time-domain signals and distance distributions with correct average distances and widths in case (A). The exact distribution in distance is shown (dashed) for 38 Å distance in (A), and it is nearly coincident with the recovered profile. The poorer SNR in (B) still enables accurate inverse reconstructions. (C) Limited time-domain data (approximately 20% of the period of the dipolar oscillation) with good SNR of 200, which is often achievable, does result in a good estimate of distance, but at the expense of broadening of $P(r)$. By rescaling the curve in (C) to 2 μs, for 20% of the period of the dipolar oscillation, an average r of about 82 Å is obtained in the $P(r)$ of panel (C). The time period of 2 μs in (A,B) is typical for nitroxide labels for proteins in most environments, but is sometimes as long as 3 to 5 μs, which permits one to record approximately a half period of dipolar oscillation for 70 – 80 Å, thus yielding a more reliable estimate of distance.

of typically 50 Å. For water-exposed labels, relaxation at longer τ is dominated by $\exp[-(2\tau/T_m)^{\kappa}]$ with $\kappa \sim 1.5$–2.5 and $T_m \sim 3$ to 4 μs (Lindgren *et al.*, 1997). This quadratic term in the exponent is governed by the nuclear spin diffusion mechanism (Milov *et al.*, 1973; Nevzorov and Freed, 2001b).

A larger κ may indicate spectral diffusion (Klauder and Anderson, 1962; Raitsimring *et al.*, 1974). This permits an r_{max} of typically ~55 to 60 Å (or ~70 – 75 Å with low accuracy).[13] Such types of relaxation could be partially suppressed by multiple refocusing and/or using deuterated solvent (Borbat *et al.*, 2004; Borbat and Freed, 2000; Jeschke *et al.*, 2004a; Milov and Tsvetkov, 1997). This could extend t_{max} to approximately 6 to 8 μs in favorable cases (Huber *et al.*, 2001), that is, much less than in D_2O/glycerol-*d*8, since there still is a bath of protons of the protein itself (Huber *et al.*, 2001). Using 6-pulse DQC helps to extend t_{max} when T_m is dominated by nuclear spin diffusion (Borbat and Freed, 2000; Borbat *et al.*, 2004). This permits a more accurate estimate of r_{max} to about 70 Å. Further improvement would require much greater effort, such as partial or complete protein deuteration, and this might extend r_{max} to 100 to 130 Å and make distances up to 80 Å much more accurate. Since such enrichment also benefits high-resolution NMR (Hamel and Dahlquist, 2005; Horst *et al.*, 2005; Venters *et al.*, 1996), one could hope that this technology may become, in the future, a standard way to improve the accuracy of distances in the 50 to 80 Å range, which are currently accessible, and to increase the sensitivity dramatically, bringing it to the micromolar level (see next section on Distance Range). This is of particular value for the difficult case of membrane proteins.

The longitudinal relaxation time, T_1, determines how frequently the pulse sequence can be repeated (usually, no more than $1.5/T_1$) and, consequently, the rate at which the data can be averaged. Both T_1 and T_2 are temperature dependent, as is the signal amplitude, which depends on the Boltzmann factor for spins in the dc magnetic field. The combined effect of all these aspects is such that for proteins in water solution or in membranes, the optimal temperature as a rule is in the range of 50 to 70 K. The presence of paramagnetic impurities with short relaxation times shortens both T_1 and T_2. This would require conducting experiments at even lower temperatures.

Distance Range

Long Distances

The ability to measure very long distances is limited by the phase memory time, T_m (see Relaxation and Sensitivity of PDS sections, pp. 75 and 79) and, for proteins, 65 to 75 Å is about the upper limit with current technology. Also, distances measured in this range are typically not very

[13] r_{max} is chosen to correspond to t_{max}, which we take as equal to one period of the dipolar oscillation $T_{dip} \equiv 2\pi/\omega_d$ (cf. Eq. (5)). Using $T_{dip}/2$ is often possible, but the accuracy in distance is less (cf. Sensitivity of PDS section, p. 79).

accurate. Modified standard methods have been shown to bring some level of improvement (Borbat *et al.*, 2004; Jeschke *et al.*, 2004a). This situation could be radically improved by protein deuteration. Alternatively, with a good spin labeling strategy, such long distances could often be avoided.

Short Distances

The π-pulse excites a spectral extent (in Gauss) of about B_1. It is necessary to excite both components of the Pake doublet in DEER, which normally uses π-pulses longer than 20 ns (B_1 of ~9 G). This provides a lower limit to DEER of approximately 15 to 20 Å (Fig. 14). However, π-pulses of 30 to 60 ns width are typical, since they provide a cleaner implementation of the method, which requires that the pump pulse and observing pulses do not overlap in spectral extent. This tends to limit DEER to 20 Å and greater. The sensitivity to shorter distances decreases significantly because the coupling increases and both components of the Pake doublet can no longer be adequately excited (Milov *et al.*, 2004). Also, account must be taken of strong dipolar coupling during these long pulses (Maryasov and Tsvetkov, 2000).

DQC uses intense pulses with B_1 of 30 G or greater; hence, it can access distances as short as about 10 Å (Fafarman *et al.*, 2007) (Fig. 14). In this case, the pseudosecular part of the dipolar term in the spin-Hamiltonian (cf. Eq. (3)) cannot be neglected (Fig. 7), but this can be accounted for in rigorous numerical simulations (Borbat and Freed, 2000). Note that for the nitroxide biradical that is aligned in a liquid crystal of Fig. 7, wherein the orientation of $\mathbf{R}_{12}$ is parallel to $\mathbf{B}_0$, the dipolar splitting is 23 MHz; (this corresponds to a 12.7 Å distance for the powder) and the $3\nu_d/2$ frequency from the pseudosecular terms (37.5 MHz) is also readily excited. The appearance of the outer splittings due to the pseudosecular term tends to broaden out the Pake doublet, thereby reducing the signal amplitude by typically a factor of ≤ 2 (in the case of short distances), which is not a significant issue since the useful signal evolution period is then usually shorter than T_m. For short distances under 20 Å, submicromolar concentrations can suffice (see next section). Also, any intermolecular contribution from singly labeled molecules in the sample is of little concern in this distance range, because the signal acquisition period is short enough that effects given by Eqs. (12–13) are small.

Thus, pulse methods could be applied to most practical cases arising in protein distance mapping. The short distance range is more appropriate, however, for organic biradicals, buried spin labels, or radical cofactors, TOAC, and similar cases, when radicals are substantially immobilized and their geometry is known or can be deduced. This range is less relevant for typical nitroxide labels with long tethers, with uncertain geometry.

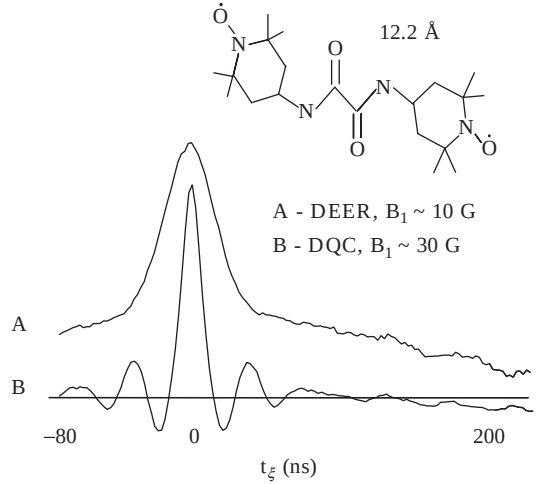

FIG. 14. The challenges of short distances. DQC and DEER were applied to a rigid 12.2 Å nitroxide biradical. Detection pulses in DEER were 16/32/32 ns, the pumping pulse was 18 ns ($B_1 \sim 10$ G). This is found to be insufficient to properly excite the dipolar spectrum. DQC using 6.2 ns π-pulse ($B_1 \sim 30$ G) develops the ~30 MHz oscillations very cleanly, similar to the case of an aligned biradical (Fig. 7). The longer pulses of DEER lead to a spread in the refocusing point of different spin packets and the weaker B_1; both smear out the high-frequency dipolar oscillations. (The biradical courtesy of R. G. Griffin.)

Optimal Range of Distances

In our experience, an optimal range of distances for the purposes of PDS is within 20 to 50 Å (45 Å for membrane proteins, whose T_m's could be in the range of 0.5–1 μs), even though larger distances can be measured with a longer period of signal averaging, but usually with reduced accuracy. Distances shorter than 20 Å introduce a relatively larger uncertainty in estimating the $C_\alpha - C_\alpha$ distances. Measurement of distances in the optimal range are fast and accurate, in most cases. The labeling sites and distance network should thus be chosen such that they provide optimal conditions for PDS, by increasing the relative number of optimal distances, as needed. Optimal conditions are not readily available for oligomeric proteins due to multiple labels and their typically large size. For an unknown structure, a preliminary scanning by several trial measurements may be very helpful.

Sensitivity of PDS

The sensitivity of pulse ESR spectroscopy is more difficult to define than for cw ESR, wherein strict criteria were established. In pulse ESR, similar criteria are harder to set, because relaxation times, which are the major determinants of the outcome of a pulse experiment, vary over a wide range

among the systems studied. For this reason, often the single-shot SNR for a standard sample (e.g., gamma-irradiated vitreous silica) can be used to calibrate sensitivity. Due to variations in pulsed ESR techniques and samples, the capacity for a meaningful experiment based on considerations of its sensitivity should be decided on a case-to-case basis (Borbat *et al.*, 1997), with all relevant parameters considered. The sensitivity of PDS techniques, specifically DQC and DEER, has been discussed in Borbat and Freed (2000), where the main criterion for sensitivity was based on the ability to perform a successful experiment (of reliably measuring a distance) in a reasonable period of time. It was chosen to correspond to an acceptable SNR, nominally taken as a S_{acc} of 10, which has to be attained in an acceptable time of experiment nominally taken as 8 h of signal averaging. Such an SNR would make it possible to obtain the distance (Fig. 13B), given a sufficient length of, t_{max} (cf. Relaxation section, p. 75), which, conservatively, should be at least one period of the dipolar oscillation. [A relaxed criterion, based on a shorter period, or even half of that, would still enable a less accurate estimate of the distance, depending on the specifics of the signal and given higher SNR than 10. This may include a priori knowledge of spin concentration and labeling efficiency or whether the distance is distributed over a narrow or broad range.] However, an S_{acc} of 10 is a bare minimum, and we usually require an SNR of at least 50, but preferably 100 to 200, to enable reliable distance distribution analysis (Chiang *et al.*, 2005b).

Even though it is possible to estimate sensitivity from first principles (Rinard *et al.*, 1999), we prefer to use an experimental calibration in the spirit of Borbat and Freed (2000), so the following approach has been chosen to give the estimates of sensitivity in distance measurements. First of all, a simple and standard experiment, such as a single-shot amplitude measurement of the primary echo, is performed under conditions when relaxation and other complications can be ignored. Then, the sensitivity of the single-shot experiment of a more complex method is deduced from this, based on the known theory of the method. Within such an approach, it suffices to measure the spin echo amplitude at a selected point of the nitroxide ESR spectrum with a two-pulse primary echo (PE) sequence, applied at a low repetition rate and with a short interpulse spacing. Such an experiment provides the SNR for a single-shot, S_1(PE), which we refer to as per unit of concentration (1 μM) or per the number of spins (1 picomole), whichever is needed. Subsequently, the S_1 for the more complex experiment is estimated from S_1(PE). Due to the limited capacity of simulating the outcome of a complex pulse sequence, such an estimate has limited accuracy, but it should be a reasonable predictor of the actual signal measurement. Finally, all the other major factors that influence the outcome of the actual experiment, such as relaxation, temperature dependence of the signal, instantaneous diffusion, or pulse sequence repetition rate,

must be determined and their values used to estimate their effect on the SNR for a given distance and its range of uncertainty.

The calibration of DQC and DEER has been conducted for our pulse ESR spectrometer (Park *et al.*, 2006) at the working frequency of 17.35 GHz on a nitroxide sample of 4-hydroxy TEMPO in a vitrified solution of 50% w/v glycerol in H_2O with a 20 μM spin concentration in a 10 μl sample volume at 70 K, where most PDS measurements are performed. The DEER calibration used a primary echo (Mims, 1965)[14] generated by $\pi/2$-π pulses (π pulse of 32 ns) separated by 80 ns, with the pulses applied at the low-field edge of the nitroxide spectrum. A similar DQC calibration was based on $\pi/2$-π pulses with a 6 ns π pulse, and the same separation as in DEER, but pulses were applied in the middle of the spectrum. For the two measurements, the ratio of the echo amplitudes (DQC versus DEER) was about 6.5 and the ratio of SNRs of the single-shot signals at the condition of optimal signal reception (given by the integration of the spin echo in the time window defined by the time points corresponding to 0.7 of the echo amplitude) was about 3.0, that is, $S_1 \approx 0.42\ \mu M^{-1}$ (DEER) and $S_1 \approx 1.25\ \mu M^{-1}$ (DQC).

Based on these numbers, the estimates of the dipolar signals for the two methods, according to the analyses given in Borbat and Freed (1999, 2000), are summarized as follows. For 4-pulse DEER with 16/32/32 ns pulses in the detection mode and a 32 ns pump pulse, S_1 is 0.084 μM^{-1}, and for DQC based on a 3/6/3/6/3/6 ns pulse sequence, S_1 is 0.3 μM^{-1}, that is, it is greater for DQC by a factor of 3.6. This ratio is supported by our experimental observations, (cf. Figs. 9–10). Using the sensitivity analysis of Borbat and Freed (2000), we estimate the SNR of the raw data[15] of the full PDS experiment as

$$SNR = 2S_1 x^2 C\eta_c K(f, T_1)(ft_{exp}/N)^{1/2}\exp(-\frac{2t_{max}}{T_m} - 2kxCGt_{max}). \qquad (17)$$

[14] The classic analysis of the SNR of a primary echo has been given by Mims, and the sensitivity in all PDS is directly related to that of a primary echo.

[15] Note that the factor of $N^{1/2}$ in Eq. (17) accounts for the effective averaging of each data point. But the raw signal can be processed in several ways in order to determine distances and the distributions in distances, when possible. In Borbat and Freed (2000), the number of points was not included in the expression for the SNR, because their sensitivity analysis was conducted within the context of the maximum measurable distances. In that case, based on consideration of spectral analysis (by FT), there should be at least $N_{min} = 4t_{max}/T_{dip}$ sampling points in order to satisfy the Nyquist criterion for the highest dipolar frequency of the Pake doublet, $2\omega_d$ (and just 2 for $t_{max} = T_{dip}/2$). It is this N_{min} that should be used as N in Eq. (17) to estimate the SNR for the dipolar spectrum in the frequency domain. Oversampling does not degrade the SNR, which is determined by the total number of signal samples (ft_{exp}) and N_{min}, but it helps to reduce aliasing in the spectrum and may have other positive effects. For reliable recovery of distributions in distances by Tikhonov analysis, 50 to 100 data points are desirable with the SNR in the data record of at least 30 (Chiang, *et al.* 2005a,b), but as has been demonstrated (cf. Fig. 13B), an SNR of 10 suffices for the case of a single distance. Equation (17) thus gives a conservative estimate.

Here, t_{exp} is the duration of the experimental data acquisition; f is the pulse sequence repetition frequency; N is the number of data points in the record; C is the doubly labeled protein concentration (μM); η_c is the ratio of the sample volume (≤ 15 μl) to that used in the calibration (10 μl). The terms in the exponent are consistent with those given in Borbat and Freed (2000), namely, the first accounts for the phase relaxation (but we use $\kappa = 1$ in Eq. (17)[16]) and the second, for instantaneous diffusion. G is method-specific (Borbat and Freed, 2000) (with its definition provided later in reference to Eqs. (18) and (18a), and for the pulse sequences defined previously, it is approximately 0.14 in DEER and approximately 0.52 in DQC. We also include the spin-labeling efficiency, x, which modifies the fraction of both spins that need to be flipped in PDS, showing its strong effect on the outcome of an experiment. In the following text, we assume complete labeling for convenience in the discussion (i.e., $x = 1$). $K(f,T_1) = [1-\exp(-1/fT_1)]$ gives the effect of incomplete spin-lattice relaxation for a given relaxation time, T_1, and repetition rate, f. (K is 0.72 for the optimal repetition rate, when $fT_1 = 0.79$ and is unity when $fT_1 \ll 1$.) As an illustration of the capability of PDS in various regimes, we consider the following examples:

Short Distances, Low Concentrations

For a short distance of 20 Å ($T_{dip} = 154$ ns), we set $t_{max} = 0.48$ μs $\approx 3T_{dip}$ in order to provide very good resolution of distance; T_m is taken as 1.0 μs, that is, the shortest within its typical range (cf. Relaxation section, p. 75); 8 ns steps in t yielding 60 data points are taken as producing the signal record; a pulse repetition frequency f of 1 kHz should be optimal for a spin-labeled protein at 70 K. One finds from Eq. (17) that just $t_{exp} \cong 4$ min of signal averaging of the DQC signal provides an SNR of 10 for a C of 1 μM. DEER will require nearly 1 h (50 min) to achieve this result. Note that this concentration corresponds to just 10 picomoles of protein. A high SNR of 100 for DQC could be attained in 6.5 h for the same amount of protein.

Long Distances

We assume $t_{max} = 4$ μs, a typical T_m of approximately 2 μs, and the steps in t are taken to be 50 ns. Then, an SNR of 10 will be reached in 8 h for a C of 2.1 μM for DQC (while for DEER, it would be 104 h). By using one period of T_{dip}, we find $R_{max} = 59$ Å ; for half of the period, R_{max} is 75 Å. (Longer distances cannot be estimated reliably with this SNR.) An accurate analysis of the distance distribution requires a higher concentration of at

[16] When $\kappa > 1$, such as for relaxation effects from nuclear spin diffusion, its partial refocusing in the DQC experiment provides an improved SNR (Borbat *et al.*, 2004).

least 10 μM in order to provide a SNR of at least 50 (Chiang *et al.*, 2005a,b), under otherwise similar conditions.

Distances in the Optimal PDS Range

We consider 50 Å as an upper limit for the "optimal" PDS distance range (cf. Distance Range section, p. 77). T_{dip} is then 2.4 μs, therefore a t_{max} of 2.4 μs suffices to provide the distance sufficiently accurate for a structure constraint. We assume the rather challenging case of $T_m = 1.5$ μs; steps in t are taken to be of 32 ns; f is 1 kHz, C is taken as 25 μM; but now we require a good SNR of 50. Such a SNR will be achieved in 16 min by DQC. DEER will require nearly 3.5 hours to achieve the same result, or else the concentration must be increased (by a factor of 2–4). Shorter distances of 20 to 45 Å are measured faster, or else yield a better SNR or resolution.

Actual Case

A recent 4-pulse DEER experiment (using a 32 ns pump pulse) conducted on 10 μM of homodimeric protein CheAΔ289 (see Distance Range section, p. 77) mutant Q545C at 60K yielded a SNR of 50 in 1.2 h of signal averaging at an f of 1.2 kHz. The phase relaxation time, T_m, was about 3.3 μs (yielding a factor of 3.7 loss of signal due to relaxation). This SNR fully supports the estimates made previously. The measured distance was approximately 40 Å, although 50 Å ($T_{dip} = 2.4$ us) is also readily accessible. Considerably longer distances could be measured for residues that are more solvent-exposed or if a deuterated buffer is used, when relaxation times could be as long as 4 to 6 μs, and consequently, a t_{max} of up to 6 μs to 8 μs can be used. We also find that, in this case, by using a t_{max} of 3.5 μs (with 32 ns steps), an SNR of 10 could be achieved for 0.5 μM of this protein in 17 h by DEER but in less than 1.5 h by DQC. This corresponds to just 5 picomoles (0.8 μg) of a 160 kDa protein in the sample, which amounts to very high absolute sensitivity.

Absolute spin sensitivity is closely related to the concentration sensitivity; however, it does increase rapidly with an increase of the working frequency due to the smaller volume of a resonator used at a higher frequency; for example, at Ku band 25 to 250 picomoles of protein are routinely used in the optimal distance range. The smaller amounts are better suited for DQC. These amounts can be reduced by about an order of magnitude using smaller resonators than we currently employ, but by an even greater factor at a higher working frequency.

We remind the reader that the previous estimates relate to our 17.3 GHz spectrometer; lower estimates of sensitivity—in particular, absolute sensitivity—would apply to the typical pulse spectrometers that operate at 9 GHz.

The practical cases encountered in the biological structure applications of PDS encompass the following ranges of experimental parameters:

(1) Average double-labeled species concentration (5–100 μM); (2) Phase relaxation times (1–4 μs); (3) Distance of interest (10–80 Å); (4) Error in distance (0.5–10 Å); (5) Acceptable SNR (10–200); (6) Data collection time (0.5–24 h). These parameters are not independent, and the requirements of (6) would not necessarily be met for any arbitrary combination of 1 through 5. However, these examples show that PDS could address most of the cases that usually occur.

Other Aspects

Although the simple form of Eqs. (7) and (10) is well-suited for practical implementation of PDS, in reality, there are many details that are of interest perhaps only to the ESR spectroscopist. Even though subtle features do appear quite often, they are usually not important for the goal of obtaining a sufficient number of distance constraints of reasonable accuracy from nitroxide-based PDS. Those that are encountered most often are noted in the following:

Orientational Selection

As was pointed out in Larsen and Singel (1993), the anisotropy of the nitroxide magnetic tensors in the general case leads to orientational selection and should not, in general, be ignored. This is especially true for DEER, in which the excitations are selective. The problem has been studied for X-band DEER by numerical methods (Maryasov *et al.*, 1998), indicating that multiple sources of broadening tend to reduce effects of correlations between the orientations of the magnetic tensors being selected by the pulses and the orientation of the interspin radial vector.

Eqs. (6) and (10) can be modified to account for orientational selection. Powder averaging then takes the form for DEER:

$$V(t) = V_0\langle G(\Omega,\Omega_1)[1 - p(\Omega,\Omega_2)(1 - \cos\omega_d(\theta,r)t]\rangle_{\Omega,\Omega_1,\Omega_2} \qquad (18)$$

and for DQC:

$$V(t) = \frac{1}{2}V_0\langle G(\Omega,\Omega_1)H(\Omega,\Omega_2)[\cos\omega_d(\theta,r)t_\xi - \cos\omega_d(\theta,r)t_m]\rangle_{\Omega,\Omega_1,\Omega_2} \qquad (18a)$$

Here, $\Omega = (\theta, \varphi)$ defines the orientation of $\mathbf{B}_0$ in the molecular frame. The z-axis of the molecular frame is selected along $\mathbf{R}_{12}$, the vector connecting the two nitroxide NO moieties, and the Euler angles $\Omega_k = (\alpha_k,\beta_k,\gamma_k)$ $(k = 1,2)$ define the orientations of the *hf* and *g*-tensors in the molecular frame for the two nitroxides (Fig. 15). G and H (or equivalently p) describe the extent of spectral excitation of spins 1 and 2, respectively[17] (Borbat and

[17] Equations 18 and 18a show only one of the two terms; the second term is obtained by permuting the subscripts 1 and 2.

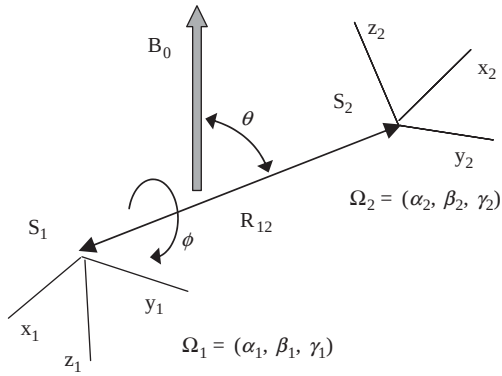

FIG. 15. The orientations of the nitroxides' magnetic tensor frames relative to the molecular frame, which is determined by the interspin vector $\mathbf{R}_{12}$.

Freed, 2000; Milov *et al.*, 2003b). The outcome of orientational selectivity is a distorted dipolar spectrum in DEER, which could result in incorrect distances emerging in the analysis based on Eqs. (6, 10, 15). DQC with its hard pulses is much less sensitive to orientational selectivity, especially when pseudosecular terms are insignificant. When desired, it can reveal the orientational correlations in considerable detail in a 2D mode of signal acquisition versus $t_\xi = t_m - 2t_p$ (Fig. 5) and versus the evolution of the spin echo time, t_2 (Borbat and Freed, 2000).

The issue of orientational selectivity is most pertinent to rigid conformations of nitroxide side-chains where $\Omega_{1,2}$ are distinct. In the case of distinct orientations (at X or Ku band), only Ω is typically used in the averaging implied by Eq. (18), and it suffices to average only over θ and to consider just β_1 and β_2 as the significant parameters (Milov *et al.*, 2003b). A particularly useful case arises for TOAC with its fixed orientation versus backbone, and it was explored in a peptide study (Milov *et al.*, 2003b). In PDS based on SDSL at working frequencies in X or Ku band, the typical side-chain flexibility, aided by unresolved inhomogeneous broadening, considerably decreases correlation effects due to partial averaging of G and H over $\Omega_{1,2}$. This is rather typical for flexible side-chain spin labels; hence, the effect hardly matters in such PDS studies. So far, in our experience, we have rarely encountered effects of orientational selectivity even for DEER for when the MTSSL is conformationally constrained.

Electron Spin-Echo Envelope Modulation (ESEEM)

Neclear ESEEM could also lead to a distorted dipolar spectrum, and in some cases interfere enough that distance determination is no longer feasible. DEER has been designed from the start to avoid ESEEM effects from magnetic nuclei. In the 3-pulse version, based on bimodal resonators and

relatively soft pulses, ESEEM from surrounding protons is virtually absent, since the excitation and detection regions of the nitroxide spectrum are well separated. In a typical implementation of 4-pulse DEER utilizing a single power amplifier at X-band and a low-Q dielectric resonator (DR) or split-ring resonator, especially when short pulses of 15 to 20 ns are used, ESEEM cannot be discounted and has to be dealt with by using suppression techniques, which have been developed for both DQC and DEER (Bonora *et al.*, 2004; Borbat *et al.*, 2002; Jeschke *et al.*, 2004a). Standard ESEEM suppression techniques are based on summing up several data records for a set of t_{m} in DQC (four collections in which t_m is stepped out by a half period of the nuclear modulation frequency), or τ' in DEER, which can be achieved with almost no loss in sensitivity. This, however, is rarely a necessity for protons in Ku-band DQC but sometimes desirable for X-band 4-pulse DEER. For Ku-band DEER, it is harder to avoid proton ESEEM due to the greater proton Zeeman frequency of ~26 MHz, but its depth is smaller by a factor of ~4 compared to X-band, and it can therefore be ignored or filtered out numerically. Deuterium modulation, however, is of greater concern in DQC even at Ku band, unless electron spin concentrations are low or t_m is sufficiently large (>4 μs).

Some Technical Aspects of DEER and DQC

A preferred setup for 3-pulse DEER is based on using two independent power amplifiers for the two frequencies (Milov *et al.*, 1981). The amplifiers should be well isolated from each other in order to avoid unwanted interference by the pulse-forming networks. Overlap of the spectral excitations induced by the two frequency sources is undesirable. This requires limiting B_1 or increasing the frequency separation; both will reduce sensitivity. It is natural to use bimodal resonators in this scheme in order to optimize sensitivity and reduce overlap between excitation profiles of pulses in pumping and detection modes. Three-pulse DEER can be conducted with a single amplifier, but this necessitates using a traveling wave tube amplifier (TWTA) in its linear regime, which is some 10 to 12 dB below the preferred saturated mode of operation. But in the linear regime, there is still some ''cross-talk'' between the pulses, even when separated in time (for example, due to memory effects via the beam current). Simultaneous application of bichromatic irradiation may also contribute a problem.

Four-pulse DEER, however, can be readily set up with a single amplifier, since the pulse of the pumping mode does not coincide with the detection pulses, and thus stronger pulses can be produced. Pulse interaction is not entirely removed but becomes less of a problem if the distance between the first two pulses is not too short. Any residual interaction can be removed by using two independent amplifiers, and both can always be operated in

their optimal regimes. Note that, in both forms of DEER, the apparent dead time (time resolution) is limited by the pulse widths, and thus is considerably longer than in DQC, which uses pulses as short as a few nanoseconds. DEER can be used without phase cycling or even with incoherent pulses. However, DEER requires high instrument stability in order to maintain gain, field, phase, etc. since all small drifts directly affect the echo amplitude, leading to low-frequency noise that could limit SNR. This requires state-of-the-art pulse generation and signal detection paths with low noise and drifts, which are difficult to achieve in a home-built instrument, unless it is designed and built with the care given by commercial equipment vendors. Figure 16 compares 3-, 4-pulse DEER, and DQC carried out in the same setup on the same sample with a single TWTA mode of operation.

A key virtue of DQC is the suppression of the large background signal (baseline) by means of its extensive phase-cycling, in particular, its use of the double-quantum filter. Unwanted modulation of the signal due to low-frequency noise and drifts in phase or gain becomes less important, thereby simplifying implementation and use. This also helps to reduce nuclear ESEEM effects, which are due mostly to modulation of the background signal from the single order coherence signals. The basic requirement is to provide reasonably accurate quadrature phase-cycling and sufficient B_1, which requires a more powerful and thus more expensive TWTA. Once these requirements are met, DQC is easy to set up and work with. Originally, the DQC experiment was conducted with a 2D-FT ESR spectrometer designed to achieve less than 30 ns dead-times with full 2 kW power in microwave pulses at a high repetition rate. This was a major instrumental challenge from the receiver protection standpoint. Since the instrumental dead-time does not need to be so short in the zero dead-time DQC technique, and repetition rates usually are low in low-temperature solids, the receiver protection is less of an issue and can be addressed by using readily available not-very-fast high-power limiters and switches. (Three- and 4-pulse DEER also have the advantage of remote echo detection and are not concerned with hard-to-obtain fast-acting receiver protection components, if the spectrometer is to be used exclusively for DEER.)

Case Study: PDS Reconstruction of Histidine Kinases Signaling Complex

Bacterial Chemotaxis

Motile bacteria move through a medium toward nutrients and away from repellents. The process that controls the motility is known as chemotaxis. In bacteria, the mechanism is based on the presence at the poles (the ends) of the bacterial cells, discoidal sensors composed of thousands of

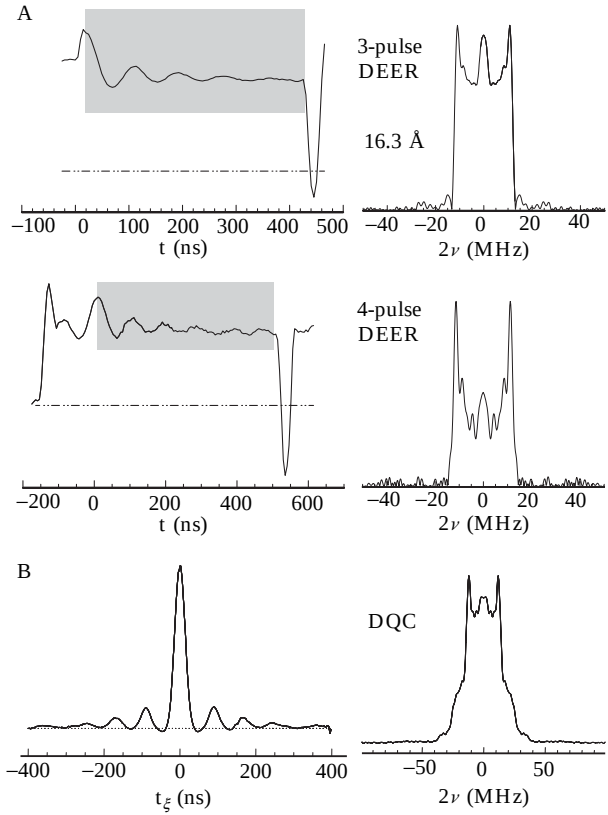

FIG. 16. (A) 3- and 4-pulse DEER, and (B) DQC (Borbat and Freed, 2000) are compared for a 16.3 Å rigid biradical in LC phase V, rapidly frozen from the isotropic phase; at −80° and 17.4 GHz. DEER was set up with a single power amplifier working in the linear regime at 10 d*B* below saturated output level. A low-Q dielectric resonator was used to accommodate the pulses at both DEER frequencies separated by ∼100 MHz. $\pi/2$ and π pulses were 10 and 20 ns in DEER and 3.2 and 6.2 ns in DQC. The pumping pulse was positioned at the low-field portion of the nitroxide spectrum. The informative parts of the signal traces in DEER are shaded. In 4-pulse DEER, the maximum of the signal is shifted in time as in DQC, so both 4-pulse DEER and DQC are zero dead-time pulse sequences. The outer turnover points of the Pake doublet are missing in the dipolar spectrum from the DEER signals. The DQC signal is considerably stronger and cleaner but decays somewhat faster due to spectral broadening caused by the pseudosecular term of the dipolar coupling. (DEER results unpublished, this lab.)

transmembrane chemical receptors of several types. They relay the effects of substrate binding over the distance of ∼250 Å to the catalytic part of the signaling complexes (Fig. 17), which are formed by the histidine

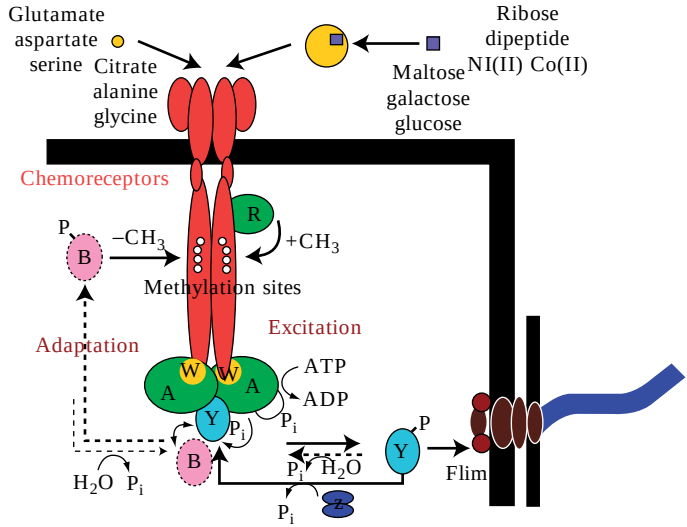

FIG. 17. The signaling bacterial receptor responds to chemical stimulants by activating histidine kinase CheA and, consequently, invoking a phosphorylation cascade that involves several other proteins. This ultimately affects the sense of rotation of the flagella motors and thus the swimming behavior. Receptors are coupled to the CheA dimers via the coupling protein CheW. A small conformational change, caused by stimulant binding at the periplasmic side of a ~300 Å long transmembrane receptor, is relayed over ~250 Å distance to the kinase at its distal cytoplasmic tip. The regulation is provided by enzymes, which (de)methylate or deamidate glutamate residues on the cytoplasmic part of the receptors. This may affect kinase activity via conformational changes of the signaling complex, cooperativity between receptors, or both, thereby changing the catalytic activity of the entire receptor array by orders of magnitude. (Adapted form Bilwes *et al.*, 2003.)

kinase CheA and the receptor-coupling protein CheW that are attached to the membrane distal ends of the cytoplasmic side of the receptors. CheW-deficient mutants exhibit disrupted chemotaxis *in vivo*. The signaling complex interacts with several soluble proteins to establish control over the sense of rotation of the flagellum motor, thus changing the swimming behavior from tumbling to direct motion. In addition, it realizes feedback control of the gain by regulating the chemotactic response to stimuli by the means of adapting the receptor complex to the concentration of attractant, thereby achieving high sensitivity and wide dynamic range (Blair, 1995; Wolanin *et al.*, 2006). Individual signaling complexes are assembled into arrays and interact with each other, enhancing the capacity of an individual signaling complex.

Objectives

Even though the bacterial chemotaxis system is, in general, well understood, the essential details of the exact functional mechanisms of its main components are still missing. The structure and functional mechanism of the entire chemotaxis receptor complex, which consists of the transmembrane receptor, histidine kinase CheA, and the coupling protein CheW, is yet to be learned, and it was our goal (Park *et al.*, 2006) to shed some light on it. There is no crystal structure of the full-length CheA, nor of CheA in a dimeric complex with CheW. CheA is a homodimer with each monomer organized into five domains P1–P5, separated by linkers of various lengths (Fig. 18). The P1 and P2 deleted protein, CheAΔ289 has a known X-ray derived structure (Bilwes *et al.*, 1999). The dimerization domain, P3, is folded into two anti-parallel α-helices. The P3 domains from the two protomers form a 4-helix bundle, which holds together the dimer. The P1 and P2 domains, separated by long flexible linkers have known X-ray structures. They are believed to have few structural constraints, although NMR work

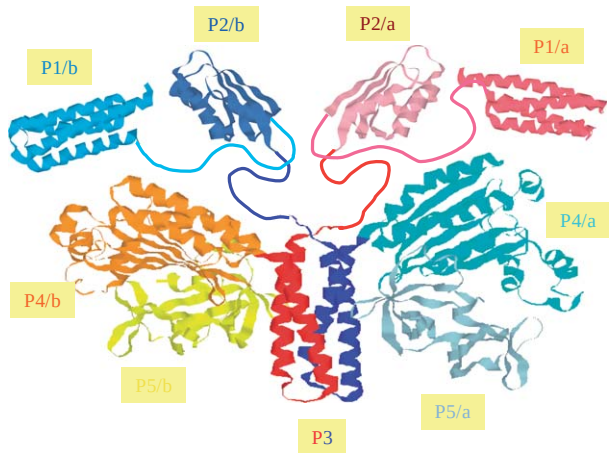

FIG. 18. A collage of the histidine kinase CheA. The whole kinase assembles as a dimer with the monomer composed of 5 domains P1–P5, connected by flexible links of various lengths. CheAΔ289 (lacking P1 and P2 domains) from *Thermotoga maritima* in the center was crystallized; P1 and P2 crystallized separately (PDB codes: 1TQG, 1U0S) were added to the figure to provide a complete view of the protein. Two P3 dimerization domains assemble into a 4-helix bundle; P4 is the catalytic domain, which phosphorylates conserved histidine of the P1 domain; P2 binds CheY or CheB, which, in turn, are phosphorylated by P1. Phosphorylated CheY(B) dissociates and controls flagella and receptor, respectively. P5 is a regulatory domain, which binds CheW and receptor and thus mediates regulation of kinase phosphotransfer activity. (Protein structure was rendered using Chime.)

in 2005 (Hamel and Dahlquist, 2005) indicates the possibility of P1 association with P4. The NMR method has provided the structure of CheW (Griswold *et al.*, 2002). Two CheW molecules bind a CheA dimer with high affinity ($K_d \sim 10$ nM), and they provide binding sites for the receptors. The structures of the cytoplasmic and periplasmic parts of several types of transmembrane receptors are available for *E. coli* and *T. maritima*.

Given the potential of accurate long-distance constraints from PDS and a ''triangulation'' approach (discussed in the next section), this methodology has been applied to the problem of bacterial chemotaxis for the first time. Initially, we had the modest goal of confirming the location of the CheW binding site, according to common belief. This implied obtaining a few distances. Nevertheless, it was decided to apply the full triangulation approach and we sought a scaffold of constraints that will orient and dock CheW with high confidence (cf. following text). Our PDS efforts have, however, developed to the point of establishing the structure of the whole signaling complex, based on our findings on the structure of the CheA/CheW complex in dilute solutions. Our efforts, synergistically combining X-ray crystallography and PDS with other biochemical methods, were reported in Park *et al.*, 2006.

Triangulation

The ''triangulation'' approach to protein mapping (Borbat *et al.*, 2002) is based on obtaining a network of distance constraints from a set of spin-labeled sites such that they uniquely define the coordinates of all (or most) of the sites. This task can be accomplished by making a sufficient number of double mutations and then measuring the distances between the respective pairs of spin labels in a ''one-at-a-time'' manner. It is not feasible, in general, to obtain distances simultaneously among several spin labels due to the flexibility of the side-chains and the structural heterogeneity of proteins, which yield fairly broad distributions in each distance. However, there can be favorable cases (Bennati *et al.*, 2005; Chiang *et al.*, 2005b) (cf. Fig. 21A). For a monomeric protein, a convenient set of labeling sites should be selected, and then a number of double mutations for this set would be made in order to produce a network of distances by PDS. A sufficiently large rigid distance network (scaffold) based on tetrahedrons (Borbat *et al.*, 2002) will strongly restrain the loci of spin labels and thereby the possible conformations of the protein (cf. Fig. 19). Building such a rigid network resembles ''triangulating'' the protein landscape. Such constraints can be used to solve the protein structure at a low resolution of 5 to 10 Å. When a very rough structure or the oligomeric state of a protein complex is of interest, a few distances may suffice (Banham *et al.*, 2006). Obtaining an

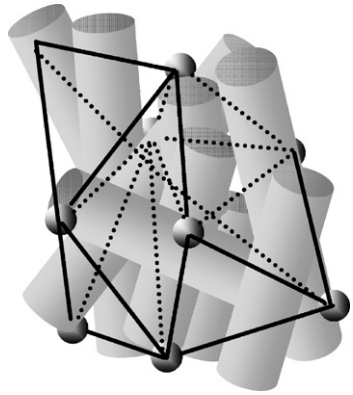

FIG. 19. A cartoon of a rigid triangulation grid based on tetrahedrons. The symbolic protein is encased into a ''cocoon'' of constraints, which uniquely define its shape and limit possible scenarios of its folds. The known secondary structure aided by homology modeling could produce a fairly accurate structure of a single protein or for it being a part of a larger complex.

accurate structure could be considerably more involved, since it could require obtaining several dozen distances in order to significantly restrain the possible conformations. The sites should be accessible for the spin-labeling reagent, and they should not alter protein structure or function; this may limit their selection. The task of site selection could be facilitated by a knowledge of the secondary structure. Site selection could be aided by nitroxide scan and/or chemical cross-linking data, which gives the information on the secondary or tertiary structure and residue exposure to solvent, thus helping to select the sites for triangulation. However, fewer than a dozen sites can produce an adequately large number of constraints (up to $N(N-1)/2$, where N is the number of sites). For this reason, there should be little concern about site availability.

Another application of this method is to determine the structure of a protein complex, (e.g., that comprised of two proteins, A and B). In this case, the triangulation grid can be based on the individual triangulation grids for each protein (grid A and grid B) and the interprotein distances (grid AB). Intraprotein grids A (and B) are obtained by the triangulation of doubly labeled proteins A (and B), whereas the interprotein grid AB is obtained using singly labeled A and B proteins. Possible structural changes of A and B, when they form the complex, could be elucidated by obtaining the grids A (and B) in the complex with the respective unlabeled ''wild-type'' (WT) partner. This is the approach that has been applied to the

problem of solving the binding structure of CheW with the P5 domain of CheAΔ289. The three grids are then used together to solve the structure of the AB complex. Clearly, this approach can be extended to multiprotein complexes and protein–RNA complexes. The task is much easier when individual protein (or their subdomains) structures are known from crystallography or NMR. However, triangulating the CheAΔ289/CheW complex is an important special case of oligomeric proteins that requires additional considerations, as will be discussed.

CheAΔ289, which is a homodimer, binds two CheWs. Its known X-ray structure indicates (an imperfect) C2 symmetry. Triangulation of a homodimeric (or, in general, oligomeric) protein is a less straightforward task than that for monomeric proteins or complexes, as has been discussed. Double mutations of protomers making up a dimer will result in having four spin labels in the dimer. Thus, four distances are possible in a dimer in the case of the C2 symmetry, and six distances are possible in general. Due to the limited capacity of PDS to resolve multiple distances (except in a few favorable cases; cf. Fig. 21A), the strategy of spin labeling or constructing the dimer should be adjusted to overcome the complications from multiple labels. One solution to this problem is to engineer dimers (or oligomers) such that they contain only one doubly labeled protomer, with the rest being WT (cf. also discussion in the Using Heterodimers, p. 104). This approach was exercised in only a few cases (cf. Using Heterodimers, p. 104) due to the difficulties of making heterodimers. The second approach, which is not necessarily applicable to all oligomeric proteins, is to select the labeling sites such that the distances between the sites on different protomers are considerably different from the intra- or interprotein distances within the protomer, thus making possible their separation.

Four mutation sites, N553, S568, D579, E646, were selected for CheA (cf. Fig. 20) on the distal end of the P5 domain surrounding the putative binding site, based on indirect studies (Bilwes *et al.*, 1999; Boukhvalova *et al.*, 2002; Hamel and Dahlquist, 2005; Shimizu *et al.*, 2000). Site selection was greatly facilitated by a knowledge of the X-ray structure of CheAΔ289. First of all, these four sites on P5 form the vertices of a sufficiently large tetrahedron with respect to which the triangle, made by the three chosen label sites (S15, S72, S80) on CheW is oriented in space, once all necessary interprotein distance measurements are made between labels on CheAΔ289 and CheW. Figure 20C shows the network of interlabel distances that we anticipated at the outset of the study. This triangulation network fixes the vertices, but it does allow for the mirror image. The knowledge of the P5 X-ray structure makes it possible to select between the two solutions. Next, we note from the known CheAΔ289 structure that

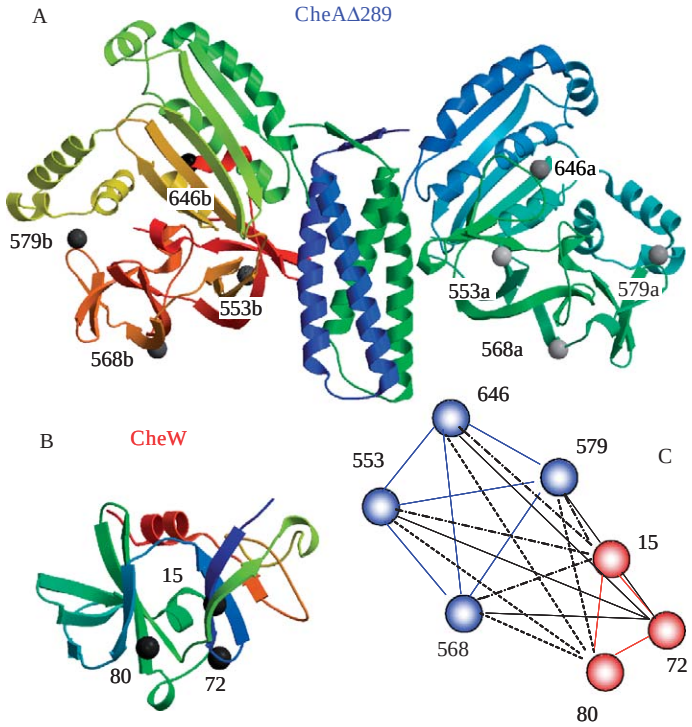

FIG. 20. Mutation sites selected for (A) CheAΔ289 (E646, S568, N553, D579) and (B) CheW (S15, S72, S80). Most of the sites are separated by more than 60Å, thus minimizing problems associated with these multi-spin cases. Additional sites were mutated at a later stage of the study in order to assess the global protein structure after two different conformations of CheAΔ354/CheW were provided by crystallography to confirm ESR-derived structure. (C) A suggested network of restraints for triangulation. Note that the putative binding site on the distal part of P5 domain detected by X-ray crystallography (Bilwes *et al.*, 1999) was under consideration here. (The structures were rendered using Mol Script.)

the distance between labeled sites on P5 of the two protomers is considerably greater (>60 Å) than that between the sites within each P5 (<40 Å), as schematically illustrated in Fig. 20A. The dipolar signal for a shorter distance exhibits much faster time evolution than that for a considerably longer distance (due to the $1/r^3$ dependence of the dipolar oscillation; cf. Eq. (5)). Consequently, they could be readily separated. Last, these four P5 sites made it possible to detect and quantify possible conformational changes in P5, as has been outlined.

All six double mutants of CheAΔ289 and all three of CheW were engineered to obtain the intraprotein set of distances (within P5 and CheW). This was carried out with and without binding of the respective wild type partner to address the possibility of change in the structure of P5 or CheW. The interprotein measurements employed the same set of mutated sites and encompassed the measurement of 12 possible distances between singly labeled CheAΔ289 and CheW. Single mutations of either CheAΔ289 or CheW were used to probe, at a later stage of study, the interdomain distances between the symmetry-related sites in the CheAΔ289 dimer and the CheAΔ289/CheW complex, with the only problem encountered being the large protein size. Most distances were expected to be in the 40 to 100 Å range. Although initially we regarded distances exceeding 60 Å as practically unmeasurable, we did find that fairly good estimates could be obtained for distances in the 60 to 80 Å range, based on reasonable assumptions regarding the time envelope of the dipolar signal and given a good SNR (cf. Fig. 13C).

Spin-Labeling and Sample Preparation

Certainly, advance knowledge of the structure of individual subunits of a large protein or complex greatly simplifies the choices of the sites for spin-labeling, as we discussed in the previous section. For a protein of unknown structure, several trial-and-error attempts would be necessary in order to establish an idea of its folds and then to refine it by further PDS measurements.

Nitroxide side chain flexibility permits a number of rotamers (Tombolato *et al.*, 2006), which can strongly deviate from the "tether-in-cone model" (Hustedt *et al.*, 2006) as was evidenced by the X-ray study of spin-labeled T4 lysozyme (Langen *et al.*, 2000). This would make it more difficult to predict the locations of the respective backbone carbons. Using different types of spin labels may help to identify the sites with nontypical conformations of side-chains; using site insensitive ones (Cai *et al.*, 2006) could help to eliminate the problem (of unusual rotamers) altogether at the expense of greater side-chain flexibility. In some cases, it is desirable to have a spatially restricted nitroxide side-chain to produce better defined distances especially for shorter distances, or else a solvent exposed site, which is easier to label and which will permit access to larger distances due to longer T_2's for such sites (Huber *et al.*, 2001). All these considerations have been appreciated in planning the study of the CheA/CheW complex. Exposed residues were selected for CheA. For CheW, the selected serine residues were distant from the conserved residues implicated in binding to CheA and they also had limited mobility, according to the NMR structure for CheW (PDB code: 1K0S).

All proteins were prepared as described elsewhere (Park *et al.*, 2006). CheAΔ289 was used for the PDS studies; the full-length CheA (which is more difficult to express) was used, in some cases, to confirm that deletion of P1 and P2 had no significant effect on the structure of the complex. (Note that for PDS, the full-length CheA does not introduce any challenge compared to the case of deletion and distances between all 9 domains could be measured.) Proteins were labeled for 4 h at 4° with 5 to 10 m*M* (1-oxyl-2,2,5,5-tetraethylpyrollinyl-3-methyl)-methanethiosulfonate (MTSSL, Toronto Research Chemicals, Toronto) in-gel filtration buffer while the His-tagged proteins were bound to nickel-nitrilotriacetic acid agarose beads. The proteins were eluted after 6 to 12 h in the presence of thrombin. Spin labeling sites are shown in Fig. 20A, as discussed in the previous section. Protein concentrations were typically in the range of 10 to 150 μM. They could not be increased considerably due to the onset of what we believe is a tendency of CheA to reversibly assemble into supramolecular constructs of unknown nature. Concentrations in the range we used usually suffice to yield clean dipolar signals for homodimeric protein, given the quantitative spin-labeling. This, however, was rarely the case, as high spin-labeling efficiency was not always achieved, especially at the early stages of the study. As a result, the concentration of double-labeled protein was a factor of 1.5 to 4 less than ideal, depending on labeling site.

As we described in the previous section, the complexes frequently involved four spin-labeled sites. For such cases, the extent of quantitative spin labeling is a complication due to an admixture of complexes bearing 3 or 4 spins, which leads to a more complex time-domain signal, especially when distances are not well separated. Magnetic dilution can sometimes be useful for oligomeric proteins, since it leads to a simpler case of mostly doubly labeled complexes (Klug and Feix, 2005; Zhou *et al.*, 2005).

In all the protein solutions, 30% w/v of glycerol was added to render the protein distribution more uniform throughout the frozen sample and to minimize possible damage to protein by water crystallization. For cryoprotection, sucrose can be used if there is any adverse reaction of protein with glycerol. But sucrose is less convenient, and we did not see any significant effect of glycerol on kinase activity or distances. The 10 to 20 μl of solutions was loaded into an 1.8 mm i.d. suprasil sample tube, plunge-frozen in liquid nitrogen, and transferred into the dielectric-resonator-based ESR probe, where it was cooled down to the working temperature in the 50 to 70 K range. Data collection times were from 10 min to 12 h, depending on concentration and distances, but were typically 30 to 120 min. Long-distance (>50 Å) measurements required using exposed sites (at least one site in the pair) deuterated solvent, and 2 to 12 h of signal averaging.

Technical Aspects

The 4-pulse DEER and 6-pulse DQC ESR methods outlined in The Newer Methods section (p. 63) were used in all cases at a frequency of 17.35 ± 0.05 GHz (corresponding to Ku band) in the two traveling-wave tube amplifier (TWTA) configuration for DEER, with only a single TWTA needed for DQC. The existing 2D-FT ESR spectrometer (Borbat *et al.*, 1997) has been modified to enable DEER by the addition of the second TWTA in order not to significantly alter its existing modes of operation and additionally to minimize interaction between the two channels. A stand-alone microwave pulse-forming channel and signal receiver for the pumping frequency had also been added, and the output pulses from the second amplifier (after passing through a rotary-vane attenuator) were simply combined with the main output by means of the 10-dB directional coupler.

A dielectric resonator coupled to a Ku-band waveguide was installed into CF935 helium flow cryostat (Oxford Instruments, Ltd.) and over-coupled to accommodate short pulses in DQC or frequency-separated pulses in DEER. $\pi/2$ and π pulses were 3.2 and 6 ns in DQC and, typically, 16 and 32 ns in DEER. The pumping pulse in DEER was in the range of 20 to 32 ns. Typically, the pumping pulse frequency, ω_B, was offset by −65 MHz from the detection frequency ω_A in order to pump at the center maximum of the nitroxide spectrum (cf. Fig. 6). At this working frequency, ESEEM from matrix protons is barely visible in DEER and is not a factor in DQC either. However, for a deuterated solvent, a weak 4 MHz ESEEM is detectable in DEER in the case of short pumping pulses and could be problematic for DQC; since a few t_m were suitable to provide blind spots (Borbat and Freed, 2000). Since spin concentrations were not very low, the sensitivity rarely was a concern, so we used DEER in most measurements, which also reduced the effects of the deuterium modulation. However, for short distances, DQC was used, and in the case of low spin concentrations, DQC often improved the SNR by a factor of 2 to 4 (cf. Fig. 10).

DEER/DQC Data and Analysis

The DQC and DEER signals were of very good quality (Fig. 21A–D). Dipolar signals from the sites on the different protomers could be distinguished and they constituted a slowly varying ''background.'' They were removed by fitting them to a second- or third-degree polynomial in the same fashion as removal of intermolecular dipolar contribution (cf. Data Processing in DQC and DEER, p. 73, and Fig. 21C). The signals isolated from the background were then Fourier transformed and, initially, the distances were estimated based on the dipolar splitting in the Pake doublets

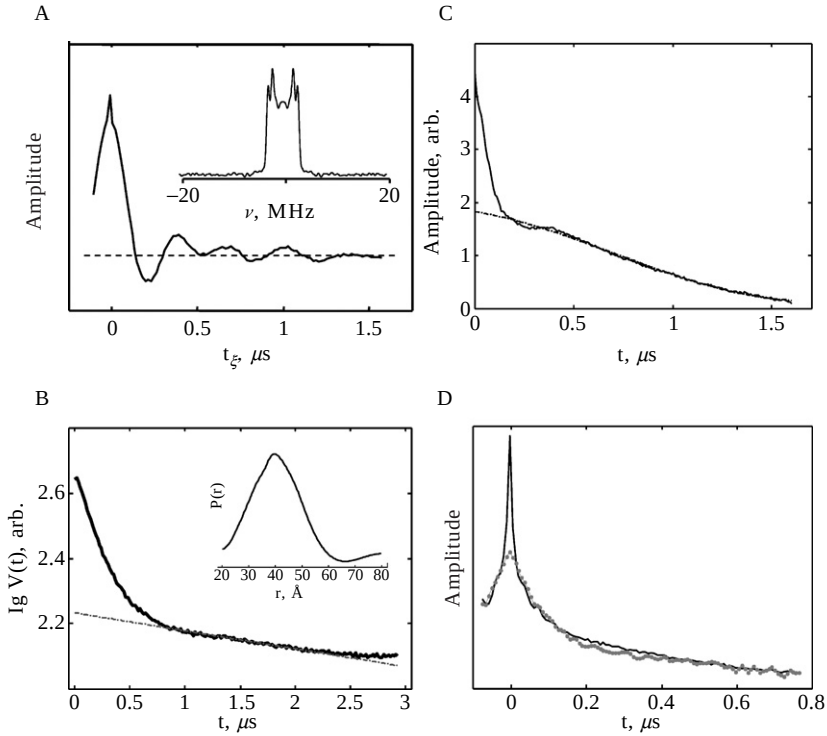

FIG. 21. Typical DQC and DEER signals obtained in the study of the CheAΔ289 complex with CheW. (A) The time-domain DQC signal for the full-length CheA labeled at S318C site on P3. 6-pulse DQC sequence was used at 17.4 GHz. Protein concentration was approximately 80 m*M*. Estimated doubly labeled protein concentration was ∼30 m*M*. Data collection time was 45 min. Inset: the dipolar spectrum is the real part of FT of the time-domain data after removing small linear baseline. Two well-defined distances of 26.3 and 28.7 Å are inferred from the two resolved singularities. They probably correspond to two distinct conformations of the P3 domain or entire CheA (Bilwes *et al.*, 1999). (B) Time-domain DEER signal for CheW complex with CheAΔ289-Q545C. Inset shows distance distribution. Concentration of CheAΔ289 was 25 μM, signal averaging time was 8 h 20 min. The latter part of the signal deviates from a straight line due to overlap of pulse excitation at the two frequencies in DEER. The signal after subtracting the background was apodized prior to L-curve Tikhonov regularization. (C) Time-domain DQC signal (solid line) for CheW80 complex with CheAΔ289-N553C. The rapidly decaying component of the signal corresponds to the distance between labels on the same monomer of CheAΔ289; the slowly decaying component of the signal originates from long distances between spin labels on different monomers. It was fitted to a third-order polynomial (dashed line) and removed (cf. DEER/DQC Data and Analysis section, p. 97). The 6-pulse DQC sequence was used at 17.4 GHz, data collection time was 22 min. (D) Time-domain DQC (solid line) and DEER (dotted line) signals from heterodimer of CheAΔ289 labeled at positions 318 and 545 in one of two protomers. The difference in signal shape is due to a greater sensitivity of the first method to short distances. Otherwise, after proper scaling, signal envelopes follow each other closely (not considering a large dc offset present in DEER data), with both reflecting rather broad distributions in distances similarly to (B).

TABLE I
INTRA- AND INTER-DOMAIN DISTANCES IN THE TRIANGULATING CHEΔ289/CHEW (PARK *ET AL.*, 2006)

Mutant	S15C	S72C	S80C	N553C	S568C	D579C	E646C
S15C		27&29[a]	18.2	37	54.5	61	43.7
S72C	X		24.5 & 30[a]	27	49	46	32.5
S80C	X	X		26	47	54.5	39.5
N553C	X	X	X		23.5	34.5	32
S568C	X	X	X	X		32.5	35.5
D579C	X	X	X	X	X		28
E646C	X	X	X	X	X	X	

[a] The second minor conformation with better defined position is likely due to an immobilized rotamer at the exposed site 72. The main component shows flexibility consistent with the type of the site.

for well-defined distances or by using half-widths of the dipolar spectra in unresolved cases. [Later, the regularization methods were used (cf. Distance Distributions section, p. 75)]. The distances between P5 and CheW and within CheW or P5 are summarized in Table I. The errors were estimated to not exceed ±2 Å, in most cases. A few of the largest distances (>50 Å) were possibly slightly biased by unwanted contributions from long distances between the sites on different protomers. The intra-protein distances were consistent with the expectations based on the CheAΔ289 X-ray structure, CheW NMR structures, and the expected geometries of the nitroxide side chains.

Complexes of double-labeled CheAΔ289 with WT CheW or vice versa probed how the complex formation perturbed the local structure. All nine possible double mutants of CheAΔ289 (6) and CheW (3) were tested. Only subtle changes in widths of distance distribution were observed in a few cases. Thus, perturbations to the local structure were smaller than the spatial resolution of the triangulation method. This justified the use of a rigid-body approach to dock CheW to P5.

Metric Matrix Distance Geometry and Rigid-Body Refinement

A set of triangulation constraints for N nitroxides can be transformed into coordinates by the metric matrix distance geometry method (Crippen and Havel, 1988), at least to determine whether the set is embeddable. One starts with the set of all possible distances d_{ik} between nitroxides i and k and constructs a rank $N-1$ metric matrix **G,** first, by placing one nitroxide at the origin, as

$$g_{ij} = (d_{i0}^2 + d_{j0}^2 - d_{ij}^2)/2 \tag{19}$$

The Gram matrix **G** is then numerically diagonalized, to give the eigensystem ($\boldsymbol{w}_i$,λ_i), with λ_i being the eigenvalues and $\boldsymbol{w}_i$ eigenvectors, respectively. The matrix **G** is

$$g_{ij} = \sum_{k=x,y,z} x_{ik}x_{jk} = \sum_{k=x,y,z} w_{ik}w_{jk}\lambda_k \tag{20}$$

with x_{ik} being Cartesian coordinates of the i-th atom. The metric matrix is positive semi-definite of rank, at most, 3. Practically, the three largest eigenvalues are used to calculate the coordinates of $N-1$ nitroxides according to

$$x_{jk} = \pm\lambda_k^{1/2} w_{jk} \tag{21}$$

where the sign is the same for all coordinates, reflecting the two mirror image-related solutions.

The method was applied with the distance information from the sites at the four positions on CheAΔ289 (N553C, D568C, E646C, S579C—all on the P5 domain) and the three CheW positions (S15C, S72C, S80C). All 12 interprotein distances and 9 intraprotein distances between 7 nitroxides (cf. Table I) were used. The CheW labeled site S15C was placed at the origin; subsequently, the metric matrix of rank 6 was generated from the other measured distances and diagonalized with a MATLAB program. The eigenvalues are (9326.1, 906.2, 509.9, 208.5, 125.9, −46.5), with the 3 smallest values being nonzero due only to measurement uncertainty. The three largest eigenvalues were used to calculate the coordinates of the four label sites on CheAΔ289 and the two remaining label sites on CheW; two possible mirror image-related coordinate sets were generated. Of the two structures, one, consistent with the relative positions of the four sites on P5, was selected. After regenerating the distance matrix from the coordinates, we found that the new distances were within 2.4 Å bounds (1.2 Å rmsd) from the experimental distances, with three distances showing larger errors (5.2 Å rmsd). A possible reason is a displacement of the E646C residue upon CheW binding and larger errors for distances above 45 Å. The resulting triangulation grid is shown in Fig. 22, and it is clear that it uniquely defines the docking of CheW.[18]

This method, in its generic form, requires all distances between the sites, and it does not consider experimental errors. There is, however, a better

[18] In Park *et al.* (2006), site 568 was not used in an otherwise similar calculation and the remaining efforts were as follows. Least square fitting among the three site coordinates calculated from distance geometry and the C_α atoms of the labeled residues on the CheAΔ289 structure and the three CheW coordinates and their corresponding positions on a rigid CheW structure (taken from the NMR ensemble) produced the complex.

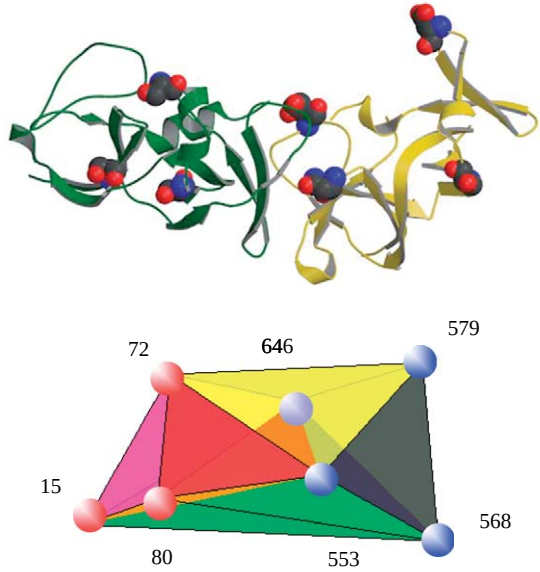

FIG. 22. (top) X-ray structure of P4/P5/CheW complex (P4 is not shown). Residues mutated to nitroxides for PDS are shown in a space-fill representation. (bottom) - Positions of nitroxide moieties found from PDS constraints correspond to that in the top figure. CheW appears to be slightly tilted and rotated about its long axis compared to the X-ray structure. The difference between X-ray and PDS is not large but cannot be discounted. Several reasons can be given: (1) the mutated residues should be replaced by nitroxide side-chains in their site-specific conformations to arrive at a better correspondence of PDS and X-ray derived structures; (2) Couplings between symmetrically positioned residues biased the long-distance constraints; (3) P4/P5/CheW was crystallized in the absence of P3, with which both CheW and P5 are expected to interact (Park *et al.*, 2006); (4) mutations at N553, and especially E646, might have had a small effect on the binding interface. Mutated sites were selected to optimize constraints in the originally presumed case of binding to the distal binding site of P5 (cf. Fig. 18), which turned out not to be the case. Thus, some chosen distances were outside the optimal range. (The ribbon structure was rendered with Mol Script; Delauney triangulation generated and rendered by MATLAB.)

method (cf. Bhatnagar *et al.*, 2007) to dock domains by rigid modeling based on the CNS software package (Brunger *et al.*, 1998), which implements the distance geometry in a more powerful way. By virtue of the implementation of distance geometry algorithms in CNS, experimental distance constraints and their uncertainties (obtained from the inverse reconstruction of time-domain data) needs to be entered. Any missing constraints could be estimated but with large errors, and thus have only minor impact on the outcome. The coordinates of the P5–CheW complex, determined by

distance geometry, have now been optimized by refinement with CNS (cf. Bhatnagar *et al.*, 2007). The PDS measured distances were treated as NMR NOE restraints. The structure was refined until convergence was achieved. To test convergence, CheW was displaced manually in various directions and the complex refined. Within rigid-body displacements of ~15 Å and rotations of ~30 degrees, the same unique solution emerged. When these methods were applied to the CheA dimer under the PDS restraints of the intersubunit P5 distances, they suggested that, in solution, P5 is slightly closer to P3, as compared to the X-ray structure of CheAΔ289. The binding site of CheW inferred from the ESR-derived structure was then confirmed by solving X-ray structure of the CheAΔ354 (Park *et al.*, 2006), which is a monomeric complex of P4–P5, with CheW.

Interdomain and Interprotein Distances in the CheW/CheAΔ289 Complex

After having solved the CheW docking issue, the global topology of CheA/CheW in dilute solution was explored. The following additional single mutations (Fig. 23) S318C (in P3), Q545C, D508C (in P5), E387C, K496C (in P4), and several double mutants shown in Table II were made for this purpose. A set of interdomain, intersubunit, and interprotein distances was generated (Table II) to explore the structure of CheAΔ289 and the CheAΔ289/CheW complex. Heterodimers were constructed in a few cases, so that intrasubunit and intersubunit distances between nonsymmetry-related

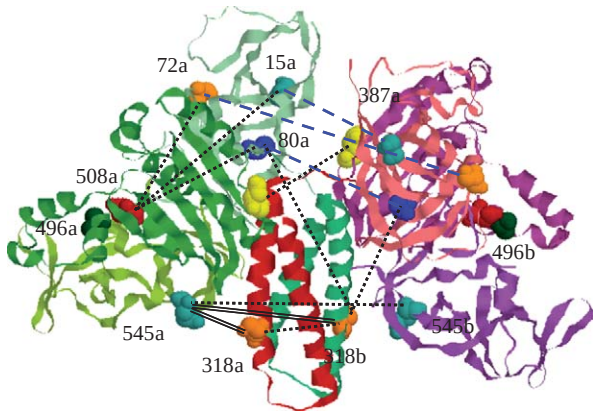

FIG. 23. Distances between several CheW mutants were measured to establish its position on the "top" of CheAΔ289. Heterodimers of P3 (S318C) and P5 (Q545C) mutants were used to establish the fixed position of the P5 domain, stabilized by interaction with P3. (Rendered with Chime.)

TABLE II
INTER-DOMAIN DISTANCES (Å) IN CHEA, CHEAΔ289, AND CHEAΔ289/CHEW COMPLEX (PARK *ET AL.*, 2006)

Domains	Residue pair[a]	Proteins in sample	Model, $C_\alpha - C_\alpha$	ESR average	ESR range
P4-P4	A387- B387	CheA[b]	42	44	30%
	A387- B387	CheA + CheW	42	46	30%
	A387- B387	CheA, full length	42	45	30%
	A496- B496	CheA	90	68[c]	30%
	A496- B496	CheA + CheW	90	N/A	
P3-P3	A318- B318	CheA	22	28	26/30[d]
	A318- B318	CheA + CheW	22	28	26/30[d]
P3-CheW	318- W80		35/44	43	30%
P4-CheW	387- W80		16/43	40–50	30%
	387- W15		17/44	40–50	30%
	387- W72		28/50	40–50	30%
P4-P5	508–646		15/65	25	22–38
P5-P5	A568- B568	CheA	76	49[c]	30%
	A568- B568	CheA + CheW	76	57[c]	30%
	A545- B545	CheA	40	41	32–50
	A545- B545	CheA + CheW	40	38	32–50
	A646- B646	CheA	62	N/A	
	A646- B646	CheA + CheW	62	61	30%
	A553- B553	CheA	63	64	30%
	A553- B553	CheA + CheW	63	N/A	
CheW-CheW	W15- W15	CheA + CheW	49	~60[c]	30%
	W80- W80	CheA + CheW	51	59–60[c]	30%
	W72- W72	CheA + CheW	70	67–70[c]	30%

[a] A and B refer to two protomers.
[b] Data for CheA289.
[c] Possible interference by aggregation.
[d] Two well-defined distances.

labels could be determined in the absence of unwanted signals from symmetry-related labels.

It was a time-consuming project, because many large distances (>50Å) were also not well defined due, in part, to the apparent freedom of the P4 and P5 domains to move about their hinges. In particular, P4 appears to exhibit substantial flexibility, as evidenced by the 387/387 data. This was not the result of deletion of P1 and P2 since similar data were obtained for full-length CheA. The P5 domain was found to be somewhat less flexible.

The broad distance distributions in Table II may have been caused, to some extent, by association of CheA dimers, which was not originally anticipated. But increasing the concentration above 500 μM indicated a

network or aggregation of unknown nature. That is, the local (as opposed to the average) spin concentration, as indicated by the intermolecular part of the DEER signal, was about triple that expected from a uniform solution and no long distances could be reliably measured. At 50 to 200 μM, a moderate flexibility of the P4 and P5 domains was observed that is probably within the amplitude of difference between subunits found in the asymmetric crystal structure (Bilwes *et al.*, 1999). Association of CheA dimers with each other via the P5 domains seen in the crystal (Bilwes *et al.*, 1999) is also supported by our PDS experiments in solutions as the protein concentration is increased. No efforts to eliminate CheA association were made other than keeping concentrations in the 50 to 100 μM range, where these additional interactions were minimized. Nevertheless, the tendency of the proteins studied to associate possibly had an impact (rather weak but non-negligible) on measured interdomain distances, in particular for those exceeding 50 Å.

The intersubunit distances between labels at residues 387 on P4, 318 on P3, and 553, 545 or 646 on P5 confirmed that the orientations of the domains of the CheAΔ289-CheW complex in solution agree well with those found in the crystal structure of CheAΔ289. Of the two structures of CheW-P5-P4 (PDB code: 2CH4), only one was supported by PDS as relevant for CheAΔ289-CheW complex, with the second possibly present as a minor conformation. The binding of two molecules of CheW to one CheAΔ289 dimer was verified by measuring the inter-CheW distances between spin labels attached to sites 15, 72, 80, and 139 in the presence of wild type CheAΔ289. All measured distances were consistent with the expectations for the reconstructed CheAΔ289-CheW complex.

An interesting finding was that the ESR distances suggest that, in solution, P5 (in both the free CheAΔ289 dimer and the CheAΔ289-CheW complex) assumes an average position relative to P3 that is slightly different but within ±10 Å of that predicted by the CheAΔ289 crystal structure. The position of P5 may well be affected by P5/P5 contacts in oligomers of CheA dimers, subject to further study.

Using Heterodimers

The position of the P3 domain relative to P5 was verified by measuring distances within CheA heterodimers in which P3 residue S318 and P5 residue Q545 were either labeled only in the same subunit or in opposite subunits. The ESR-measured intrasubunit and intersubunit distances between 318 and 545 correlated well with separations in the CheAΔ289 dimer measured by X-rays (Table III). Heterodimers offer a useful approach for detailed ESR mapping of oligomeric proteins. Ideally, one constructs the

TABLE III
INTER-DOMAIN DISTANCES (Å) IN HETERODIMERS OF CHEAΔ289 AND IN THE COMPLEX WITH CHEW (PARK *ET AL.*, 2006)

Domains	Residue pair	Proteins in sample	Model, $C_\alpha - C_\alpha$	ESR average	ESR range
P5-P3	A545- A318	CheAHD	12	14	12–30
	A545- A318	CheAHD + CheW	12	14	12–30
	A545- B318	CheAHD	30	30	

complex to have only two labels (e.g., both spin labels on only one protomer, or one spin label each on two protomers in well-defined locations in the complex). Heterodimers can be expressed as tandem constructs (Liu *et al.*, 2001); however, this methodology is not simple, and it may fail to express or fold the protein properly. Alternatively, one has to dissociate the protein and reassemble it into the heterodimer when this is at all possible. CheAΔ289 does dissociate at elevated temperatures, and this property was applied to engineer heterodimers with spin labels on the same or opposite subunits. To do so, CheAΔ289 mutants, double-labeled at 318 and 545 sites (Fig. 23), after incubation at 65° with the wild type carrying the histidine tag were recombined and labeled on a nickel affinity column. Magnetic dilution is sometimes a useful approach to studying oligomeric proteins (Klug and Feix, 2005). Spin labeling of different subunits required some level of magnetic dilution (by a factor of 3 to 5) of histidine-tagged mutants with WT to keep the fraction of multi-spin complexes much lower than that of complexes with two spins. This led to increased fraction of single labeled complex.[19]

Discussion and Perspective

We have described a successful application of PDS to the study of bacterial chemotaxis. It has led to a new perspective into the possible organization of the receptor signaling array (Fig. 24), which is substantially different from what had previously been suggested for the *E. coli* receptor (Shimizu *et al.*, 2000). This new perspective remains to be tested. The outcome of the structural study on just the CheAΔ289/CheW complex (Park *et al.*, 2006) by PDS led to a new proposal for the entire signaling complex. The capabilities of PDS are currently being directed to the

[19] This procedure could have been carried out rigorously only by using a multiple affinity approach (tandem purification based on having different tags of opposite protomers in the dimer), which was not attempted.

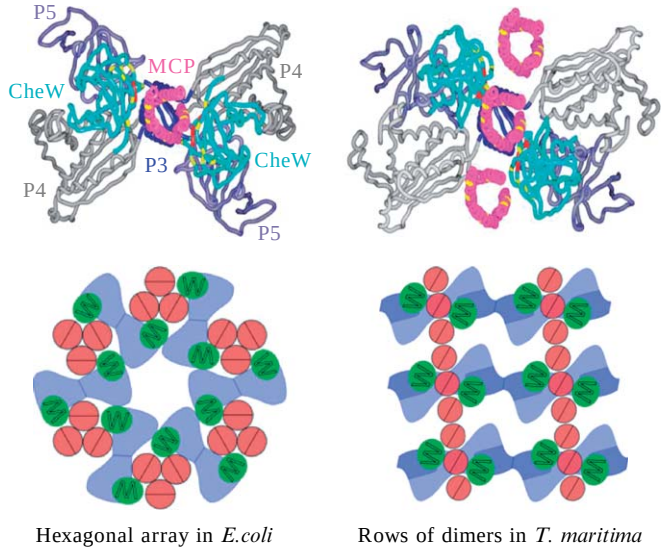

FIG. 24. Receptor–kinase interactions. In *T. maritima,* the methyl-accepting domain of the receptor forms dimers that are 225 Å long, with a diameter of ~20Å (Park *et al.*, 2006). The canyon formed by two CheW molecules sitting on top of a CheAΔ289 dimer is wide enough to accommodate one receptor dimer. Two additional receptor dimers can be positioned on either side of the center receptor giving a stoichiometry of three receptor dimers to one CheA dimer and two CheWs. The bottom figures compare two possible type of receptor arrays. (Adapted from Weis, 2006.)

reconstruction of the entire signaling complex of the receptor, which will test this proposal.

In most PDS studies conducted thus far, just a few distances were typically obtained, often with the goal of detecting an important structural change or establishing the oligomerization state. On the other hand, cw ESR routinely employs extensive protein scans (Crane *et al.*, 2005; Cuello *et al.*, 2004; Dong *et al.*, 2005) to elucidate aspects of secondary and tertiary structures. PDS is certainly capable of extensive protein mapping, as we have demonstrated (Borbat *et al.*, 2006; Park *et al.*, 2006). In all, at least 70 distances (including those using WT proteins) have been obtained as the work on CheA/CheW progressed. In retrospect, such a massive effort of PDS could be compressed into 2 to 4 weeks of continuous operation, given that all the samples are prepared. This is, by any measure, quite a short period of time. With good labeling strategy, extensive mapping based on 20 to 50 distances could be completed in about a week, that is, as fast as an

ESR nitroxide scan. The method can be applied to a variety of structural problems that are currently difficult to address by other methods. The main hurdles for PDS are the conformational heterogeneity of proteins; flexibility of the tether of the nitroxide spin label; and oligomeric proteins yielding multiple spin systems, for which there are workarounds, but they remain to be developed into standard techniques. PDS offers spatial resolution that is intermediate between cryo EM and atomic-level resolution methods, although it currently lacks the capacity of sorting out structurally heterogeneous objects as single-particle cryo EM is able to (Stark and Lührmann, 2006; Sigworth, 2007). Functional or conserved cysteines constitute another problem needing solution.

Although PDS may successfully be performed with nanomole or even picomole (at higher working frequency) amount of protein (in the microgram range), extensive study may consume a larger amount. This includes the need to make several different mutants and to account for losses during purification and spin-labeling of the target biomolecule. However, this is still far less than is usually needed to obtain a complete 3D structure by the major methods, although modern NMR is constantly improving its detection limits (as is also true of crystallography), but it often requires expensive isotopic substitution. Also, the procedure of SDSL is well developed and is relatively fast and inexpensive. In the future, it also could be fully automated. After protein purification and nitroxide labeling, the sample is cryopreserved, thereby mitigating difficulties arising from limited protein stability. There is also substantial potential to increase the throughput by perfecting the PDS techniques.

The minuscule amounts of protein that are needed for PDS may well be in line with expected future developments of incorporating unnatural amino-acid targets for selective labeling by suitable (novel) spin-labeling reagents. Attainable improvements in sample preparation (particularly labeling) will allow PDS to address small scales and protein samples that suffer from low-level expression. This could help to reduce the overall costs of using deuterated solvents, lipids, detergents, and proteins that benefit the method. In addition, expected further improvements in pulse ESR instrumentation directed toward enhancing sensitivity to enable the study of even smaller amounts of labeled protein and to increase throughput should further benefit PDS.

At present, protein structure can be reasonably accurately evaluated using just self-consistent nitroxide side-chain modeling (as has been noted) and by structure refinement by CNS for a sufficiently large set of ESR distance constraints (cf. Ch. 4). One could anticipate that future developments will enable ESR distance restraints combined with homology

modeling, nitroxide side-chain geometry simulation, and structure prediction to be applied to generate detailed 3D structures of large proteins and their complexes.

Concluding Remarks

PDS has so far been successfully applied on a relatively small scale to a variety of systems in the context of structure and function, and it has the potential to address a wider range of issues. The successful application of PDS triangulation to determine the ternary structure of the CheA/CheW complex of *T. maritima* demonstrates the viability of the method and sets the stage for its future applications in this category. A similar mapping effort has focused on the helix topology of α-Synuclein (Borbat *et al.*, 2006).

In this chapter, we have stressed the point that PDS is a rather straightforward technique in its principles and implementation, and is not overburdened with complexities. We have tried to convey our enthusiasm that PDS will develop into a standard technique for structure determination, given that it does have several virtues, which should lead to its wider acceptance.

Acknowledgments

We thank Brian Crane for a critical reading of the manuscript, Alexandrine Bilwes and Jaya Bhatnagar for help with figures and data processing, and Sang Park for developing the methods for CheA labeling and for metric matrix distance geometry. We also thank Boris Dzikovski, Robert G. Griffin, Igor Grigoriev, Gunnar Jeschke, Anup Upadhyay, and Zheng Zhou for kindly providing samples for PDS. We thank Diane Patzer and Joanne Trutko for their extensive help with the manuscript preparation. This work was supported by grants from the NIH/NCRR P41-RR016292 and NIH/NIBIB EB03150.

References

Abragam, A. (1961). ''The Principles of Nuclear Magnetism,'' pp. 103–105. Clarendon Press, Oxford, UK.

Altenbach, C. A., Flitsch, S. L., Khorana, H. G., and Hubbell, W. L. (1989). Structural studies on transmembrane proteins. 2. Spin labeling of bacteriorhodopsin mutants at unique cysteines. *Biochemistry* **28,** 7806–7812.

Altenbach, C. A., Marti, T., Khorana, H. G., and Hubbell, W. L. (1990). Transmembrane protein structure: Spin labeling of bacteriorhodopsin mutants. *Science* **248,** 1088.

Altenbach, C. A., Oh, K.-J., Trabanino, R. J., Hideg, K., and Hubbell, W. L. (2001). Estimation of inter-residue distances in spin labeled proteins at physiological temperatures: Experimental strategies and practical limitations. *Biochemistry* **40,** 15471–15482.

Astashkin, A. V., Kodera, Y., and Kawamori, A. (1994). Distance between tyrosines Z+ and D+ in plant Photosystem II as determined by pulsed EPR. *Biochim. Biophys. Acta* **1187,** 89–93.

Banham, J. E., Timmel, C. R., Abbott, R. J. M., Lea, S. M., and Jeschke, G. (2006). The characterization of weak protein–protein interactions: Evidence from DEER for the trimerization of a von Willebrand factor A domain in solution. *Angewandte Chemie, International Edition* **45,** 1058–1061.

Bartucci, R., Erilov, D. A., Guzzi, R., Sportelli, L., Dzuba, S. A., and Marsh, D. (2006). Time-resolved electron spin resonance studies of spin-labelled lipids in membranes. *Chem. Phys. Lipids* **141,** 142–157.

Becker, J. S., and Saxena, S. (2005). Double quantum coherence electron spin resonance on coupled Cu(II)–Cu(II) electron spins. *Chem. Phys. Lett.* **414,** 248–252.

Bennati, M., Robblee, J. H., Mugnaini, V., Stubbe, J., Freed, J. H., and Borbat, P. P. (2005). EPR distance measurements support a model for long-range radical initiation in *E. coli* ribonucleotide reductase. *J. Am. Chem. Soc.* **127,** 15014–15015.

Bennati, M., Weber, A., Antonic, J., Perlstein, D. L., Robblee, J., and Stubbe, J. (2003). Pulsed ELDOR spectroscopy measures the distance between the two tyrosyl radicals in the r2 subunit of the *E. coli* ribonucleotide reductase. *J. Am. Chem. Soc.* **125,** 14988–14989.

Berliner, L. J., Eaton, G. R., and Eaton, S. S. (2000). ''Distance Measurements in Biological Systems by EPR.'' Kluwer Academic, NY.

Bhatnagar, J., Freed, J. H., and Crane, B. R. (2006). Rigid body refinement of protein complexes with long-range distance restraints from pulsed dipolar ESR. *Methods in Enzymology* **423,** 117–133.

Biglino, D., Schmidt, P. P., Reijerse, E. J., and Lubitz, W. (2007). PELDOR study on the tyrosyl radicals in the R2 protein of mouse ribonucleotide reductase. *Chem. Phys. Chem.* **8,** 58–62.

Bilwes, A. M., Alex, L. A., Crane, B. R., and Simon, M. I. (1999). Structure of CheA, a signal-transducing histidine kinase. *Cell* **96,** 131–141.

Bilwes, A. M., Park, S. Y., Quezada, C. M., Simon, M. I., and Crane, B. R. (2003). *In* ''Structure and Functions of CheA, the Histidine Kinase Central to Bacterial Chemotaxis in Histidine Kinase in Signal Transduction.'' (M. Inoue and R. Dutta, eds.), Chapter 4, pp. 47–72. Academic Press, NY.

Blair, D. F. (1995). How bacteria sense and swim. *Ann. Rev. Microbiol.* **49,** 489–522.

Bonora, M., Becker, J., and Saxena, S. (2004). Suppression of electron spin-echo envelope modulation peaks in double quantum coherence electron spin resonance. *J. Magn. Reson.* **170,** 278–283.

Borbat, P., Ramlall, T. F., Freed, J. H., and Eliezer, D. (2006). Inter-helix distances in lysophospholipid micelle-bound a-synuclein from pulsed ESR measurements. *J. Am. Chem. Soc.* **128,** 10004–10005.

Borbat, P. P., Crepeau, R. H., and Freed, J. H. (1997). Multifrequency two-dimensional Fourier transform ESR: An X/Ku-band spectrometer. *J. Magn. Reson.* **127,** 155–167.

Borbat, P. P., da Costa-Filho, A. J., Earle, K. A., Moscicki, J. K., and Freed, J. H. (2001). Electron spin resonance in studies of membranes and proteins. *Science* **291,** 266–269.

Borbat, P. P., Davis, J. H., Butcher, S. E., and Freed, J. H. (2004). Measurement of large distances in biomolecules using double-quantum filtered refocused electron spin-echoes. *J. Am. Chem. Soc.* **126,** 7746–7747.

Borbat, P. P., and Freed, J. H. (1999). Multiple-quantum ESR and distance measurements. *Chem. Phys. Lett.* **313,** 145–154.

Borbat, P. P., and Freed, J. H. (2000). *In* ''Biological Magnetic Resonance'' (L. J. Berliner, G. R. Eaton, and S. S. Eaton, eds.), Vol. 19, pp. 383–459. Kluwer Academic, NY.

Borbat, P. P., Mchaourab, H. S., and Freed, J. H. (2002). Protein structure determination using long-distance constraints from double-quantum coherence ESR: Study of T4-lysozyme. *J. Am. Chem. Soc.* **124,** 5304–5314.

Borovykh, I. V., Ceola, S., Gajula, P., Gast, P., Steinhoff, H.-J., and Huber, M. (2006). Distance between a native cofactor and a spin label in the reaction center of Rhodobacter

sphaeroides by a two-frequency pulsed electron paramagnetic resonance method and molecular dynamics simulations. *J. Magn. Reson.* **180,** 178–185.

Boukhvalova, M. S., Dahlquist, F. W., and Stewart, R. C. (2002). CheW binding interactions with CheA and Tar: Importance for chemotaxis signaling in *Escherichia coli*. *J. Biol. Chem.* **277,** 22251–22259.

Bowers, P. M., Strauss, C. E. M., and Baker, D. (2000). *De novo* protein structure determination using sparse NMR data. *J. Biomol. NMR* **19,** 311–318.

Bowman, M. K., Maryasov, A. G., Kim, N., and deRose, V. J. (2004). Visualization of distance distribution from pulsed double electron–electron resonance data. *App. Magn. Reson.* sb: volume-nr>26, , 23–39.

Brunger, A. T., Adams, P. D., Clore, G. M., DeLano, W. L., Gros, P., Grosse-Kunstleve, R. W., Jiang, J.-S., Kuszewski, J., Nilges, M., Pannu, N. S., Read, R. J., Rice, L. M., *et al.* (1998). Crystallography and NMR System: A new software suite for macromolecular structure determination. *Acta Crystallographica, Section D: Biological Crystallography* **D54,** 905–921.

Cai, Q., Kusnetzow, A. K., Hubbell, W. L., Haworth, I. S., Gacho, G. P. C., Van Eps, N., Hideg, K., Chambers, E. J., and Qin, P. Z. (2006). Site-directed spin labeling measurements of nanometer distances in nucleic acids using a sequence-independent nitroxide probe. *Nucleic Acids Res.* **34,** 4722–4730.

Chandrasekhar, S. (1943). Stochastic problems in physics and astronomy. *Rev. Modern Phys.* **15,** 1.

Chiang, Y.-W., Borbat, P. P., and Freed, J. H. (2005a). The determination of pair distance distributions by pulsed ESR using Tikhonov regularization. *J. Magn. Reson.* **172,** 279–295.

Chiang, Y.-W., Borbat, P. P., and Freed, J. H. (2005b). Maximum entropy: A complement to Tikhonov regularization for determination of pair distance distributions by pulsed ESR. *J. Magn. Reson.* **177,** 184–196.

Codd, R., Astashkin, A. V., Pacheco, A., Raitsimring, A. M., and Enemark, J. H. (2002). Pulsed ELDOR spectroscopy of the Mo(V)/Fe(III) state of sulfite oxidase prepared by one-electron reduction with Ti(III) citrate. *JBIC, J. Biol. Inorg. Chem.* **7,** 338–350.

Columbus, L., and Hubbell, W. L. (2002). A new spin on protein dynamics. *Trends Biochem. Sci.* **27,** 288–295.

Columbus, L., Kalai, T., Jekoe, J., Hideg, K., and Hubbell, W. L. (2001). Molecular motion of spin labeled side chains in a-helices: Analysis by variation of side chain structure. *Biochemistry* **40,** 3828–3846.

Cornish, V. W., Benson, D. R., Altenbach, C. A., Hideg, K., Hubbell, W. L., and Schultz, P. G. (1994). Site-specific incorporation of biophysical probes into proteins. *Proc. Natl. Acad. Sci. USA* **91,** 2910–2914.

Crane, J. M., Mao, C., Lilly, A. A., Smith, V. F., Suo, Y., Hubbell, W. L., and Randall, L. L. (2005). Mapping of the docking of SecA onto the chaperone SecB by site-directed spin labeling: Insight into the mechanism of ligand transfer during protein export. *J. Mol. Biol.* **353,** 295–307.

Crippen, G. M., and Havel, T. F. (1988). ''Distance Geometry and Molecular Conformation.'' John Wiley & Sons, New York, NY.

Cuello, L. G., Cortes, D. M., and Perozo, E. (2004). Molecular architecture of the KvAP voltage-dependent K+ channel in a lipid bilayer. *Science (Washington, DC, United States)* **306,** 491–495.

Denysenkov, V. P., Prisner, T. F., Stubbe, J., and Bennati, M. (2006). High-field pulsed electron-electron double resonance spectroscopy to determine the orientation of the tyrosyl radicals in ribonucleotide reductase. *Proc. Natl. Acad. Sci. USA* **103,** 13386–13390.

Dong, J., Yang, G., and Mchaourab, H. S. (2005). Structural basis of energy transduction in the transport cycle of MsbA. *Science (Washington, DC, United States)* **308,** 1023–1028.

Dzikovski, B. G., Borbat, P. P., and Freed, J. H. (2004). Spin-labeled gramicidin A: Channel formation and dissociation. *Biophys. J.* **87,** 3504–3517.

Dzuba, S. A. (2005). Pulsed EPR structural studies in the nanometer range of distances. *Russ. Chem. Rev.* **74,** 619–637.

Elsaesser, C., Brecht, M., and Bittl, R. (2002). Pulsed electron-electron double resonance on multinuclear metal clusters: Assignment of spin projection factors based on the dipolar interaction. *J. Am. Chem. Soc.* **124,** 12606–12611.

Fafarman, A. T., Borbat, P. P., Freed, J. H., and Kirshenbaum, K. (2007). Characterizing the structure and dynamics of folded oligomers: Pulsed ESR studies of peptoid helices. *Chemical Communications (Cambridge, United Kingdom)* **4,** 377–379.

Fajer, P. G. (2005). Site-directed spin labeling and pulsed dipolar electron paramagnetic resonance (double electron-electron resonance) of force activation in muscle. *J. Phys. Condens. Matter* **17,** S1459–S1469.

Fanucci, G. E., and Cafiso, D. S. (2006). Recent advances and applications of site-directed spin labeling. *Curr. Opin. Struct. Biol.* **16,** 644–653.

Farahbakhsh, Z. T., Altenbach, C. A., and Hubbell, W. L. (1992). Spin labeled cysteines as sensors for protein–lipid interaction and conformation in rhodopsin. *Photochem. Photobiol.* **56,** 1019–1033.

Freed, J. H. (2000). New technologies in electron spin resonance. *Annu. Rev. Phys. Chem.* **51,** 655–689.

Fu, Z., Aronoff-Spencer, E., Backer, J. M., and Gerfen, G. J. (2003). The structure of the inter-SH2 domain of class IA phosphoinositide 3-kinase determined by site-directed spin labeling EPR and homology modeling. *Proc. Natl. Acad. Sci. USA* **100,** 3275–3280.

Griswold, I. J., Zhou, H., Matison, M., Swanson, R. V., McIntosh, L. P., Simon, M. I., and Dahlquist, F. W. (2002). The solution structure and interactions of CheW from *Thermotoga maritima*. *Nature Struct. Biol.* **9,** 121–125.

Hamel, D. J., and Dahlquist, F. W. (2005). The contact interface of a 120 kD CheA-CheW complex by methyl TROSY interaction spectroscopy. *J. Am. Chem. Soc.* **127,** 9676–9677.

Hanson, P., Anderson, D. J., Martinez, G., Millhauser, G., Formaggio, F., Crisma, M., Toniolo, C., and Vita, C. (1998). Electron spin resonance and structural analysis of water soluble, alanine-rich peptides incorporating TOAC. *Mol. Phys.* **95,** 957–966.

Hanson, P., Millhauser, G., Formaggio, F., Crisma, M., and Toniolo, C. (1996). ESR characterization of hexameric, helical peptides using double TOAC spin labeling. *J. Am. Chem. Soc.* **118,** 7618–7625.

Hilger, D., Jung, H., Padan, E., Wegener, C., Vogel, K.-P., Steinhoff, H.-J., and Jeschke, G. (2005). Assessing oligomerization of membrane proteins by four-pulse DEER: pH-dependent dimerization of NhaA Na+/H+ antiporter of *E. coli*. *Biophys. J.* **89,** 1328–1338.

Horst, R., Bertelsen, E. B., Fiaux, J., Wider, G., Horwich, A. L., and Wuthrich, K. (2005). Direct NMR observation of a substrate protein bound to the chaperonin GroEL. *Proc. Natl. Acad. Sci. USA* **102,** 12748–12753.

Hubbell, W. L., and Altenbach, C. (1994). Investigation of structure and dynamics in membrane proteins using site-directed spin labeling. *Curr. Opin. Struct. Biol.* **4,** 566–573.

Hubbell, W. L., Cafiso, D. S., and Altenbach, C. (2000). Identifying conformational changes with site-directed spin labeling. *Nature Struct. Biol.* **7,** 735–739.

Huber, M., Lindgren, M., Hammarstrom, P., Martensson, L.-G., Carlsson, U., Eaton, G. R., and Eaton, S. S. (2001). Phase memory relaxation times of spin labels in human carbonic anhydrase II: Pulsed EPR to determine spin label location. *Biophys. Chem.* **94,** 245–256.

Hustedt, E. J., Smirnov, A. I., Laub, C. F., Cobb, C. E., and Beth, A. H. (1997). Molecular distances from dipolar coupled spin-labels: The global analysis of multifrequency continuous wave electron paramagnetic resonance data. *Biophys. J.* **72,** 1861–1877.

Hustedt, E. J., Stein, R. A., Sethaphong, L., Brandon, S., Zhou, Z., and DeSensi, S. C. (2006). Dipolar coupling between nitroxide spin labels: The development and application of a tether-in-a-cone model. *Biophys. J.* **90,** 340–356.

Jeschke, G. (2002). Distance measurements in the nanometer range by pulse EPR. *Chemphyschem. Europ. J. Chem. Phys. Phys. Chem.* **3,** 927–932.

Jeschke, G., Bender, A., Paulsen, H., Zimmermann, H., and Godt, A. (2004a). Sensitivity enhancement in pulse EPR distance measurements. *J. Magn. Reson.* **169,** 1–12.

Jeschke, G., Koch, A., Jonas, U., and Godt, A. (2002). Direct conversion of EPR dipolar time evolution data to distance distributions. *J. Magn. Reson.* **155,** 72–82.

Jeschke, G., Panek, G., Godt, A., Bender, A., and Paulsen, H. (2004b). Data analysis procedures for pulse ELDOR measurements of broad distance distributions. *Appl. Magn. Reson.* **26,** 223–244.

Jeschke, G., Pannier, M., Godt, A., and Spiess, H. W. (2000). Dipolar spectroscopy and spin alignment in electron paramagnetic resonance. *Chem. Phys. Lett.* **331,** 243–252.

Jeschke, G., and Schlick, S. (2006). Spatial distribution of stabilizer-derived nitroxide radicals during thermal degradation of poly(acrylonitrile-butadiene-styrene) copolymers: A unified picture from pulsed ELDOR and ESR imaging. *Phys. Chem. Chem. Phys.* **8,** 4095–4103.

Jeschke, G., and Spiess, H. W. (2006). Distance measurements in solid-state NMR and EPR spectroscopy. *In* ''Novel NMR and EPR Techniques,'' pp. 21–63. Springer, Berlin.

Jeschke, G., Wegener, C., Nietschke, M., Jung, H., and Steinhoff, H.-J. (2004c). Interresidual distance determination by four-pulse double electron-electron resonance in an integral membrane protein: The Na+/proline transporter PutP of *Escherichia coli*. *Biophys. J.* **86,** 2551–2557.

Kay, C. W. M., Elsaesser, C., Bittl, R., Farrell, S. R., and Thorpe, C. (2006). Determination of the distance between the two neutral flavin radicals in augmenter of liver regeneration by pulsed ELDOR. *J. Am. Chem. Soc.* **128,** 76–77.

Klauder, J. R., and Anderson, P. W. (1962). Spectral diffusion decay in spin resonance experiments. *Phys. Rev.* **125,** 912–932.

Klug, C. S., and Feix, J. B. (2005). SDSL: A survey of biological applications. Chapter 10. *In* ''Biological Magnetic Resonance'' (S. S. Eaton, G. R. Eaton, and L. J. Berliner, eds.), Vol. 24, pp. 269–308. Kluwer, NY.

Klug, C. S., Camenisch, T. G., Hubbell, W. L., and Hyde, J. S. (2005). Multiquantum EPR spectroscopy of spin-labeled arrestin K267C at 35 GHz. *Biophys. J.* **88,** 3641–3647.

Koteiche, H. A., and Mchaourab, H. S. (1999). Folding pattern of the a-crystallin domain in aA-crystallin determined by site-directed spin labeling. *J. Mol. Biol.* **294,** 561–577.

Kulik, L. V., Dzuba, S. A., Grigoryev, I. A., and Tsvetkov, Y. D. (2001). Electron dipole–dipole interaction in ESEEM of nitroxide biradicals. *Chem. Phys. Lett.* **343,** 315–324.

Kulik, L. V., Grishin, Y. A., Dzuba, S. A., Grigoryev, I. A., Klyatskaya, S. V., Vasilevsky, S. F., and Tsvetkov, Y. D. (2002). Electron dipole-dipole ESEEM in field-step ELDOR of nitroxide biradicals. *J. Magn. Reson.* **157,** 61–68.

Kurshev, V. V., Raitsimring, A. M., and Tsvetkov, Y. D. (1989). Selection of dipolar interaction by the ''2 + 1'' pulse train ESE. *J. Magn. Reson. (1969–1992)* **81,** 441–454.

Langen, R., Oh, K. J., Cascio, D., and Hubbell, W. L. (2000). Crystal structures of spin labeled T4 lysozyme mutants: Implications for the interpretation of EPR spectra in terms of structure. *Biochemistry* **39,** 8396–8405.

Larsen, R. G., and Singel, D. J. (1993). Double electron-electron resonance spin-echo modulation: Spectroscopic measurement of electron spin pair separations in orientationally disordered solids. *J. Chem. Phys.* **98,** 5134–5146.

Lindgren, M., Eaton, G. R., Eaton, S. S., Jonsson, B.-H., Hammarstrom, P., Svensson, M., and Carlsson, U. (1997). Electron spin echo decay as a probe of aminoxyl environment in spin-labeled mutants of human carbonic anhydrase II. *Journal of the Chemical Society, Perkin Transactions* **2,** 2549–2554.

Liu, Y. S., Somponpisut, P., and Perozo, E. (2001). Structure of the KcsA channel intracellular gate in the open state. *Nat. Struct. Biol.* **8,** 883–887.

Maryasov, A. G., and Tsvetkov, Y. D. (2000). Formation of the pulsed electron-electron double resonance signal in the case of a finite amplitude of microwave fields. *Appl. Magn. Reson.* **18,** 583–605.

Maryasov, A. G., Tsvetkov, Y. D., and Raap, J. (1998). Weakly coupled radical pairs in solids. ELDOR in ESE structure studies. *Appl. Magn. Reson.* **14,** 101–113.

Mchaourab, H. S., Kalai, T., Hideg, K., and Hubbell, W. L. (1999). Motion of spin-labeled side chains in T4 lysozyme: Effect of side chain structure. *Biochemistry* **38,** 2947–2955.

Mchaourab, H. S., Oh, K. J., Fang, C. J., and Hubbell, W. L. (1997). Conformation of T4 lysozyme in solution. Hinge-bending motion and the substrate-induced conformational transition studied by site-directed spin labeling. *Biochemistry* **36,** 307–316.

McNulty, J. C., Silapie, J. L., Carnevali, M., Farrar, C. T., Griffin, R. G., Formaggio, F., Crisma, M., Toniolo, C., and Millhauser, G. L. (2001). Electron spin resonance of TOAC labeled peptides: Folding transitions and high frequency spectroscopy. *Biopolymers* **55,** 479–485.

Milov, A. D., Erilov, D. A., Salnikov, E. S., Tsvetkov, Y. D., Formaggio, F., Toniolo, C., and Raap, J. (2005). Structure and spatial distribution of the spin-labeled lipopeptide trichogin GA IV in a phospholipid membrane studied by pulsed electron-electron double resonance (PELDOR). *Phys. Chem. Chem. Phys.* **7,** 1794–1799.

Milov, A. D., Naumov, B. D., and Tsvetkov, Y. D. (2004). The effect of microwave pulse duration on the distance distribution function between spin labels obtained by PELDOR data analysis. *Appl. Magn. Reson.* **26,** 587–599.

Milov, A. D., Maryasov, A. G., and Tsvetkov, Y. D. (1998). Pulsed electron double resonance (PELDOR) and its applications in free-radicals research. *Appl. Magn. Reson.* **15,** 107–143.

Milov, A. D., Maryasov, A. G., Tsvetkov, Y. D., and Raap, J. (1999). Pulsed ELDOR in spin-labeled polypeptides. *Chem. Phys. Lett.* **303,** 135–143.

Milov, A. D., Ponomarev, A. B., and Tsvetkov, Y. D. (1984). Electron-electron double resonance in electron spin echo: Model biradical systems and the sensitized photolysis of decalin. *Chem. Phys. Lett.* **110,** 67–72.

Milov, A. D., Salikhov, K. M., and Shirov, M. D. (1981). Application of the double resonance method to electron spin echo in a study of the spatial distribution of paramagnetic centers in solids. *Soviet Physics-Solid State* **23,** 565–569.

Milov, A. D., Salikhov, K. M., and Tsvetkov, Y. D. (1973). Phase relaxation of hydrogen atoms stabilized in an amorphous matrix. *Soviet Physics–Solid State* **15,** 802–806.

Milov, A. D., and Tsvetkov, Y. D. (1997). Double electron-electron resonance in electron spin echo. Conformations of spin-labeled poly-4-vinylpyridine in glassy solutions. *Appl. Magn. Reson.* **12,** 495–504.

Milov, A. D., Tsvetkov, Y. D., Formaggio, F., Crisma, M., Toniolo, C., and Raap, J. (2000a). Self-assembling properties of membrane-modifying peptides studied by PELDOR and CW-ESR spectroscopies. *J. Am. Chem. Soc.* **122,** 3843–3848.

Milov, A. D., Tsvetkov, Y. D., Formaggio, F., Crisma, M., Toniolo, C., and Raap, J. (2001). The secondary structure of a membrane-modifying peptide in a supramolecular

assembly studied by PELDOR and CW-ESR spectroscopies. *J. Am. Chem. Soc.* **123,** 3784–3789.

Milov, A. D., Tsvetkov, Y. D., Formaggio, F., Crisma, M., Toniolo, C., and Raap, J. (2003a). Self-assembling and membrane modifying properties of a lipopeptaibol studied by CW-ESR and PELDOR spectroscopies. *J. Peptide Sci.* **9,** 690–700.

Milov, A. D., Tsvetkov, Y. D., Formaggio, F., Oancea, S., Toniolo, C., and Raap, J. (2003b). Aggregation of spin labeled trichogin GA IV dimers: Distance distribution between spin labels in frozen solutions by PELDOR data. *J. Phy. Chem. B* **107,** 13719–13727.

Milov, A. D., Tsvetkov, Y. D., and Raap, J. (2000b). Aggregation of trichogin analogs in weakly polar solvents: PELDOR and ESR studies. *Appl. Magn. Reson.* **19,** 215–226.

Mims, W. B. (1965). Electron echo methods in spin resonance spectrometry. *Rev. Sci. Instrum.* **36,** 1472–1479.

Narr, E., Godt, A., and Jeschke, G. (2002). Selective measurements of a nitroxide–nitroxide separation of 5 nm and a nitroxide–copper separation of 2.5 nm in a terpyridine-based copper(II) complex by pulse EPR spectroscopy. *Angewandte Chemie, International Edition* **41,** 3907–3910.

Nevzorov, A. A., and Freed, J. H. (2001a). Direct-product formalism for calculating magnetic resonance signals in many-body systems of interacting spins. *J. Chem. Phys.* **115,** 2401–2415.

Nevzorov, A. A., and Freed, J. H. (2001b). A many-body analysis of the effects of the matrix protons and their diffusional motion on electron spin resonance line shapes and electron spin echoes. *J. Chem. Phys.* **115,** 2416–2429.

Ottemann, K. M., Xiao, W., Shin, Y.-K., and Koshland, D. E., Jr. (1999). A piston model for transmembrane signaling of the aspartate receptor. *Science (Washington, D. C.)* **285,** 1751–1754.

Pake, G. E. (1948). Nuclear resonance absorption in hydrated crystals: Fine structure of the proton line. *J. Chem. Phys.* **16,** 327–336.

Pannier, M., Veit, S., Godt, A., Jeschke, G., and Spiess, H. W. (2000). Dead-time free measurement of dipole–dipole interactions between electron spins. *J. Magn. Reson.* **142,** 331–340.

Park, S.-Y., Borbat, P. P., Gonzalez-Bonet, G., Bhatnagar, J., Pollard, A. M., Freed, J. H., Bilwes, A. M., and Crane, B. R. (2006). Reconstruction of the chemotaxis receptor–kinase assembly. *Nature Struct. Mol. Biol.* **13,** 400–407.

Persson, M., Harbridge, J. R., Hammarstrom, P., Mitri, R., Martensson, L.-G., Carlsson, U., Eaton, G. R., and Eaton, S. S. (2001). Comparison of electron paramagnetic resonance methods to determine distances between spin labels on human carbonic anhydrase II. *Biophys. J.* **80,** 2886–2897.

Pfannebecker, V., Klos, H., Hubrich, M., Volkmer, T., Heuer, A., Wiesner, U., and Spiess, H. W. (1996). Determination of end-to-end distances in oligomers by pulsed EPR. *J. Phys. Chem.* **100,** 13428–13432.

Prisner, T., Rohrer, M., and MacMillan, F. (2001). Pulsed EPR spectroscopy: Biological applications. *Annu. Rev. Phys. Chem.* **52,** 279–313.

Pusep, A. Y., and Shokhirev, N. V. (1984). Application of a singular expansion in the analysis of spectroscopic inverse problems. *Optika I spectroscopia* **57,** 792–798.

Rabenstein, M. D., and Shin, Y.-K. (1995). Determination of the distance between two spin labels attached to a macromolecule. *Proc. Natl. Acad. Sci. USA* **92,** 8239–8243.

Rabenstein, M. D., and Shin, Y.-K. (1996). HIV-1 gp41 tertiary structure studied by EPR spectroscopy. *Biochemistry* **35,** 13922–13928.

Raitsimring, A. M., Peisach, J., Lee, H. C., and Chen, X. (1992). Measurement of distance distribution between spin labels in spin-labeled hemoglobin using an electron spin echo method. *J. Phys. Chem.* **96,** 3526–3531.

Raitsimring, A. M., and Salikhov, K. M. (1985). Electron spin echo method as used to analyze the spatial distribution of paramagnetic centers. *Bull. Magn. Reson.* **7,** 184–217.

Raitsimring, A. M., Salikhov, K. M., Umanskii, B. A., and Tsvetkov, Y. D. (1974). Instantaneous diffusion in the electron spin echo of paramagnetic centers stabilized in solid matrixes. *Fizika Tverdogo Tela (Sankt-Peterburg)* **16,** 756–766.

Rakowsky, M. H., Zecevic, A., Eaton, G. R., and Eaton, S. S. (1998). Determination of high-spin iron(III)-nitroxyl distances in spin-labeled porphyrins by time-domain EPR. *J. Magn. Reson.* **131,** 97–110.

Rinard, G. A., Quine, R. W., Song, R., Eaton, G. R., and Eaton, S. S. (1999). Absolute EPR spin echo and noise intensities. *J. Magn. Reson.* **140,** 69–83.

Ruthstein, S., Potapov, A., Raitsimring, A. M., and Goldfarb, D. (2005). Double electron-electron resonance as a method for characterization of micelles. *J. Phys. Chem. B* **109,** 22843–22851.

Sale, K., Sar, C., Sharp, K. A., Hideg, K., and Fajer, P. G. (2002). Structural determination of spin label immobilization and orientation: A Monte Carlo minimization approach. *J. Magn. Reson.* **156,** 104–112.

Sale, K., Song, L., Liu, Y.-S., Perozo, E., and Fajer, P. (2005). Explicit treatment of spin labels in modeling of distance constraints from dipolar EPR and DEER. *J. Am. Chem. Soc.* **127,** 9334–9335.

Salikhov, K. M., Dzyuba, S. A., and Raitsimring, A. (1981). The theory of electron spin-echo signal decay resulting from dipole–dipole interactions between paramagnetic centers in solids. *J. Magn. Reson.* **42,** 255–276.

Schiemann, O., Piton, N., Mu, Y., Stock, G., Engels, J. W., and Prisner, T. F. (2004). A PELDOR-based nanometer distance ruler for oligonucleotides. *J. Am. Chem. Soc.* **126,** 5722–5729.

Seiter, M., Budker, V., Du, J.-L., Eaton, G. R., and Eaton, S. S. (1998). Interspin distances determined by time domain EPR of spin-labeled high-spin methemoglobin. *Inorg. Chim. Acta* **273,** 354–366.

Shimizu, T. S., Le Novere, N., Levin, M. D., Beavil, A. J., Sutton, B. J., and Bray, D. (2000). Molecular model of a lattice of signaling proteins involved in bacterial chemotaxis. *Nature Cell Biol.* **2,** 792–796.

Sigworth, F. J. (2007). From cryo-EM multiple protein stuctures in one shot. *Nature methods* **4,** 20–21.

Slichter, C. P. (1990). ''Principles of Magnetic Resonance.'' Springer-Verlag, Berlin-Heidelberg-New York.

Stark, H., and Lührmann, R. (2006). Cyro-electron microscopy of spliceosomal components. *Annu. Rev. Biophys. Biomol. Struct.* **35,** 435–457.

Steinhoff, H.-J. (2004). Inter- and intra-molecular distances determined by EPR spectroscopy and site-directed spin labeling reveal protein–protein and protein–oligonucleotide interaction. *Biol. Chem.* **385,** 913–920.

Tombolato, F., Ferrarini, A., and Freed, J. H. (2006). Modeling the effects of structure and dynamics of the nitroxide side chain on the ESR spectra of spin-labeled proteins. *J. Phys. Chem. B* **110,** 26260–26271.

Venters, R. A., Farmer, B. T., II, Fierke, C. A., and Spicer, L. D. (1996). Characterizing the use of perdeuteration in NMR studies of large proteins: 13C, 15N, and 1H assignments of human carbonic anhydrase II. *J. Mol. Biol.* **264,** 1101–1116.

Weis, R. M. (2006). Inch by inch, row by row. *Nat. Struct. Mol. Biol.* **13,** 382–384.

Wolanin, P. M., Baker, M. D., Francis, N. R., Thomas, D. R., DeRosier, D. J., and Stock, J. B. (2006). Self-assembly of receptor/signaling complexes in bacterial chemotaxis. *Proc. Natl. Acad. Sci. USA* **103,** 14313–14318.

Xiao, W., Poirier, M. A., Bennett, M. K., and Shin, Y.-K. (2001). The neuronal t-SNARE complex is a parallel four-helix bundle. *Nature Struct. Biol.* **8,** 308–311.

Xu, Q., Ellena, J. F., Kim, M., and Cafiso, D. S. (2006). Substrate-dependent unfolding of the energy coupling motif of a membrane transport protein determined by double electron-electron resonance. *Biochemistry* **45,** 10847–10854.

Zecevic, A., Eaton, G. R., Eaton, S. S., and Lindgren, M. (1998). Dephasing of electron spin echoes for nitroxyl radicals in glassy solvents by non-methyl and methyl protons. *Mol. Phys.* **95,** 1255–1263.

Zhou, Z., DeSensi, S. C., Stein, R. A., Brandon, S., Dixit, M., McArdle, E. J., Warren, E. M., Kroh, H. K., Song, L., Cobb, C. E., Hustedt, E. J., and Beth, A. H. (2005). Solution structure of the cytoplasmic domain of erythrocyte membrane band 3 determined by site-directed spin labeling. *Biochemistry* **44,** 15115–15128.